Cold-water corals and hydrocarbon-rich seepage in the Pompeia Province (Gulf of Cádiz) — living on the edge

Blanca Rincón-Tomás[1], Jan-Peter Duda[2], Luis Somoza[3], Francisco Javier González[3], Dominik Schneider[1], Teresa Medialdea[3], Esther Santofimia[4], Enrique López-Pamo[4], Pedro Madureira[5], Michael Hoppert[1], and Joachim Reitner[6,7]

[1]Georg-August-University Göttingen, Institute of Microbiology and Genetics, Grisebachstraße 8, 37077 Göttingen, Germany
[2]Department of Earth Sciences, University of California Riverside, CA 92521, USA
[3]Marine Geology Dept., Geological Survey of Spain, IGME, Ríos Rosas 23, 28003 Madrid, Spain
[4]Geological Resources Dept., Geological Survey of Spain, IGME, Ríos Rosas 23, 28003 Madrid, Spain
[5]Estrutura de Missão para a Extensão da Plataforma Continental (EMEPC). Rua Costa Pinto 165, 2770-047 Paço de Arcos, Portugal
[6]Georg-August-University Göttingen, Göttingen Centre of Geosciences, Goldschmidtstraße 3, 37077 Göttingen, Germany
[7]Göttingen Academy of Sciences and Humanities, Theaterstraße 7, 37073 Göttingen, Germany

Correspondence to: Blanca Rincón-Tomás (b.rincontomas@gmail.com)

Abstract. Azooxanthellate cold-water corals (CWCs) have a global distribution and have commonly been found in areas of active fluid seepage. The relationship between the CWCs and these fluids, however, is not well understood. This study aims at unraveling the relationship between CWC development and hydrocarbon-rich seepage in the Pompeia Province (Gulf of Cádiz, Atlantic Ocean). This region comprises mud volcanoes, coral ridges and fields of coral mounds, which are all affected by the tectonically driven seepage of hydrocarbon-rich fluids. The type of seepage such as focused, scattered, diffused or eruptive, is tightly controlled by a complex system of faults and diapirs. Early diagenetic carbonates from the currently active Al Gacel MV exhibit δ^{13}C-signatures down to -28.77 ‰ VPDB, indicating biologically derived methane as the main carbon source. The same samples contain ^{13}C-depleted lipid biomarkers diagnostic for archaea such as crocetane (δ^{13}C down to -101.2 ‰ VPDB) and PMI (δ^{13}C down to -102.9 ‰ VPDB), evidencing microbially mediated anaerobic oxidation of methane (AOM). This is further supported by next generation DNA sequencing data, demonstrating the presence of AOM related microorganisms (ANME archaea, sulfate-reducing bacteria) in the carbonate. Embedded corals in some of the carbonates and CWC fragments exhibit less negative δ^{13}C values (-8.08 to -1.39‰ VPDB), pointing against the use of methane as the carbon source. Likewise, the absence of DNA from methane- and sulfide-oxidizing microbes in a sampled coral does not support a chemosynthetic lifestyle of these organisms. In the light of these findings, it appears that the CWCs benefit rather indirectly from hydrocarbon-rich seepage by using methane-derived authigenic carbonates as a substratum for colonization. At the same time, chemosynthetic organisms at active sites, such as Siboglinidae worms, prevent coral dissolution and necrosis by feeding on the seeping fluids (i. e. methane, sulfate, hydrogen sulfide), allowing cold-water corals to colonize carbonates currently affected by hydrocarbon-rich seepage.

1. Introduction

Cold-water corals (CWCs) are a widespread, non-phylogenetic group of cnidarians that include hard skeleton scleractinian corals, soft-tissue octocorals, gold corals, black corals and hydrocorals (Roberts et al., 2006; Roberts

41   et al., 2009; Cordes et al., 2016). Typically, they thrive at low temperatures $(4 - 12\,°C)$ and occur in water depths

42   of ca. $50 - 4000$ m. CWCs are azooxanthellate and solely rely on their nutrition as energy and carbon sources

43   (Roberts et al., 2009). Some scleractinian corals (e.g. *Lophelia pertusa, Madrepora oculata, Dendrophyllia*

44   *cornigera, Dendrophyllia alternata, Eguchipsammia cornucopia*) are able to form colonies or even large carbonate

45   mounds (Rogers et al., 1999; Wienberg et al., 2009; Watling et al., 2011; Somoza et al., 2014). Large vertical

46   mounds and elongated ridges formed by episodic growth of scleractinian corals (mainly *Lophelia pertusa*) are for

47   instance widely distributed along the continental margins of the Atlantic Ocean (Roberts et al., 2009). These

48   systems are of great ecological value since they offer sites for resting-, breeding-, and feeding for various

49   invertebrates and fishes (Cordes et al., 2016 and references therein).

50   Several environmental forces influence the initial settling, growth, and decline of CWCs. These include, among

51   others, an availability of suitable substrates for coral larvae settlement, low sedimentation rates, oceanographic

52   boundary conditions (e.g. salinity, temperature and density of the ocean water) and a sufficient supply of nutrients

53   through topographically controlled currents systems (Mortensen et al., 2001; Roberts et al., 2003; Thiem et al.,

54   2006; Dorschel et al., 2007; Dullo et al., 2008; Van Rooij et al., 2011; Hebbeln et al., 2016). Alternatively, the

55   "hydraulic theory" suggests that CWC ecosystems may be directly fueled by fluid seepage, providing a source of

56   e.g. sulfur compounds, nitrogen compounds, P, CO_2 and/or hydrocarbons (Hovland, 1990; Hovland and Thomsen,

57   1997; Hovland et al., 1998; 2012). This relationship is supported by the common co-occurrence of CWC-mounds

58   and hydrocarbon-rich seeps around the world, for example at the Hikurangi Margin in New Zealand (Liebetrau et

59   al., 2010), the Brazil margin (e.g. Gomes-Sumida et al., 2004), the Darwin Mounds in the northern Rockall Trough

60   (Huvenne et al., 2009), the Kristin field on the Norwegian shelf (Hovland et al., 2012), the western Alborán Sea

61   (Margreth et al., 2011), and the Gulf of Cádiz (e.g. Díaz-del-Río et al., 2003; Foubert et al., 2008). However,

62   CWCs may also benefit rather indirectly from seepage. For instance, methane-derived authigenic carbonates

63   (MDACs) formed through the microbially mediated anaerobic oxidation of methane (AOM; Suess & Whiticar,

64   1989; Hinrichs et al., 1999; Thiel et al., 1999; Boetius et al., 2000; Hinrichs & Boetius, 2002) potentially provide

65   hard substrata for larval settlement (e.g. Díaz-del-Rio et al., 2003; Van Rooij et al., 2011; Magalhães et al. 2012;

66   Le Bris et al., 2016; Rueda et al., 2016). In addition, larger hydrocarbon-rich seepage related structures such as

67   mud volcanoes and carbonate mud mounds act as morphological barriers favoring turbulent water currents that

68   deliver nutrients to the corals (Roberts et al., 2009; Wienberg et al., 2009; Margreth et al., 2011; Vandorpe et al.,

69   2016).

70   In the Gulf of Cádiz, most CWC occurrences are "coral graveyards" with only a few living corals that are situated

71   along the Iberian and Moroccan margins. These CWC systems are typically associated with diapiric ridges, steep

72   fault-controlled escarpments, and mud volcanoes (MVs) such as the Faro MV, Hesperides MV, Mekness MV, and

73   mud volcanoes in the Pen Duick Mud Volcano Province (Foubert et al., 2008; Wienberg et al., 2009). Mud

74   volcanoes (and other conspicuous morphological structures in this region such as pockmarks) are formed through

75   tectonically induced fluid flow (Pinheiro et al., 2003; Somoza et al., 2003; Medialdea et al., 2009; León et al.,

76   2010; 2012). The fluid flow is promoted through the of the high regional tectonic activity and high fluid contents

77   of sediments in this area (mainly CH_4 and, to a lesser extent, H_2S, CO_2, and N_2: Pinheiro et al., 2003; Hensen et

78   al., 2007; Scholz et al., 2009; Smith et al., 2010; González et al., 2012). However, the exact influence of fluid flow

79   on CWC growth in this region remains elusive.

80   This study aims at elucidating the impact of hydrocarbon-rich seepage on CWCs, by testing whether or not CWCs
81   in our working area have a chemosynthetic lifestyle, as well as outdrawing further ecological benefits and
82   drawbacks of seepage-related processes for CWCs. We address our hypothesis by the combined analyses of high-
83   resolution ROV underwater images, geophysical data (e.g. seabed topography, deep high-resolution multichannel
84   seismic reflection data), and sample materials (water analysis, petrographic features, δ^{13}C- and δ^{18}O-signatures of
85   carbonates, lipid biomarkers and environmental 16s rDNA sequences of the prokaryotic microbial community).
86   We focus our study in the Pompeia Province (**Fig. 1**), which encompasses mud volcanoes as the currently active
87   Al Gacel MV (León et al., 2012), diapiric coral ridges and mounds. Based on our findings, we propose an
88   integrated model to explain the tempo-spatial and genetic relations between CWCs, chemosynthetic fauna and
89   hydrocarbon-rich seepage in the study area.

2. Materials and Methods

91   This study is based on data and samples from the Pompeia Province that were collected during the Subvent-2
92   cruise in 2014 aboard the R/V Sarmiento de Gamboa (**Fig. 1**). In order to elucidate the tempo-spatial and genetic
93   relations between CWCs, chemosynthetic fauna and hydrocarbon-rich seepage in this area, we explored geological
94   features (mud volcanoes and coral ridges) by means of underwater imaging and geophysical data. ROV dives were
95   carried out at the Al Gacel MV (D10 and D11) and the Northern Pompeia Coral Ridge (D03). Subsequently, we
96   conducted detailed analyses on selected samples from sites that were characterized by different types of seepage
97   during sampling (**Table 1**). Samples from the Al Gacel MV include authigenic carbonates (D10-R3, D10-R7, D11-
98   R8), pore-water from the sediment (via micro-cores; D10-C5, D10-C8, D11-C10), and water from above the
99   seafloor (via Niskin bottles; D10-N12, D11-N9). Furthermore, a scleractinian coral fragment was recovered from
100   the Northern Pompeia Coral Ridge (D03-B1). All samples were immediately stored at room temperature
101   (petrographic analysis), 4 °C (water, sediments and pore-water analysis), −20 °C (stable isotopic analysis), or −80
102   °C (environmental DNA analysis).

2.1. Geophysical survey

104   Seabed topography of the studied sites was mapped by using an Atlas Hydrosweep DS (15 kHz and 320 beams)
105   multibeam echosounder (MBES). Simultaneously, ultra-high resolution sub-bottom profiles were acquired with
106   an Atlas Parasound P-35 parametric chirp profiler (0.5 − 6 kHz). Deep high-resolution multichannel seismic
107   reflection data was obtained using an array of 7 SERCEL gi-guns (system composed of 250 + 150 + 110 + 45
108   cubic inches) with a total of 860 cubic inches. The obtained data were recorded with an active streamer
109   (SIG®16.3x40.175; 150 m length with 3 sections of 40 hydrophones each). The shot interval was 6 seconds and
110   the recording length 5 seconds two-way travel time (TWT). Data processing (filtering and stacking) was performed
111   on board with Hot Shots software.

2.2. Video survey and analysis

113   A remotely operated vehicle (ROV-6000 Luso, operated by EMEPC) was used for photographic documentation
114   (high definition digital camera, 1024x1024 pixel) and sampling. The ROV was further equipped with a STD/CTD-
115   SD204 sensor (*in-situ* measurements of salinity, temperature, oxygen, conductivity, sound velocity and depth),

116 HydroC^{TM} sensors (*in-situ* measurements of CO_2 and CH_4), Niskin bottles (CH_4 concentrations, pH and redox

117 potential measurements), and a ROV core sampler (up to 16 cm).

2.2.1. Seawater and pore-water analysis

119 Niskin water-samples and micro-cores covering the water/sediment interface were recovered from an active

120 pockmark close to the summit of the Al Gacel MV (D10-N4, D10-C5, D10-C8; same site as carbonate-sample

121 D10-R7) as well as directly from its summit (D11-N9, D11-C10). Redox potentials (ORP) and pH-values of the

122 water contained in the Niskin bottles were measured on site with HANNA portable instruments (HI 9025). Pore-

123 water from the micro-cores was immediately extracted by centrifuging 10 cm thick slices of the sediments. Upon

124 extraction, the pore-water was filtered with syringe filters of cellulose acetate (0.2 μm pore), acidified with distilled

125 nitric acid (HNO_3), and stored under 4 °C before further analysis. Major and trace elements were subsequently

126 measured with an Agilent 7500c inductively coupled plasma mass spectrometer (ICP-MS). Method accuracy and

127 precision was checked by external standards (MIV, EPA, NASC, CASS). The precision was better than 5 % RSD

128 (residual standard deviation) and the accuracy better than 4%. Concentrations of S^{2-} were measured with a Hanch-

129 Lange DR 2800 spectrophotometer (cuvette test kit LCK 653).

2.3. Petrographic analysis

131 General petrographic analysis was performed on thin sections (ca. 60 μm thickness) with a Zeiss SteREO

132 Discovery.V8 stereomicroscope (transmitted- and reflected light) linked to an AxioCam MRc 5-megapixel camera.

133 Additional detailed petrographic analysis of textural and mineralogical features was conducted on polished thin

134 sections (ca. 30 μm thickness) using a DM2700P Leica Microscope coupled to a DFC550 digital camera.

135 Carbonate textures have been classified following Dunham (1962) and Embry & Klovan (1971).

2.4. Stable isotope signatures ($\delta^{13}C$, $\delta^{18}O$) of carbonates

137 Stable carbon and oxygen isotope measurements were conducted on ca. 0.7 mg carbonate powder obtained with a

138 high precision drill (ø 0.8 mm). The analyses were performed with a Thermo Scientific Kiel IV carbonate device

139 coupled to a Finnigan Delta Plus gas isotope mass spectrometer. Accuracy and reproducibility were checked

140 through the replicate analysis of a standard (NBS19) and reproducibility was better than 0.1 ‰. Stable carbon and

141 oxygen isotope values are expressed in the standard δ notation as per mill (‰) deviations relative to Vienna Pee

142 Dee Belemnite (VPDB).

2.5. Lipid biomarker analysis

2.5.1. Sample preparation

145 All materials used were pre-combusted (500 °C for >3 h) and/or extensively rinsed with acetone prior to sample

146 contact. A laboratory blank (pre-combusted sea sand) was prepared and analyzed in parallel to monitor laboratory

147 contaminations.

148 The preparation and extraction of lipid biomarkers was conducted in orientation to descriptions in Birgel et al.

149 (2006). Briefly, the samples were first carefully crushed with a hammer and internal parts were powdered with a

150 pebble mill (Retsch MM 301, Haan, Germany). Hydrochloric acid (HCl; 10 %) was slowly poured on the powdered

151 samples which were covered with dichloromethane (DCM)-cleaned water. After 24 h of reaction, the residues (pH

152 3 − 5) were repeatedly washed with water and then lyophilized.

153 3 g of each residue was saponified with potassium hydroxide (KOH; 6 %) in methanol (MeOH). The residues were

154 then extracted with methanol (40 mL, 2x) and, upon treatment with HCl (10 %) to pH 1, in DCM (40 mL, 2x) by

155 using ultra-sonication. The combined supernatants were partitioned in DCM vs. water (3x). The total organic

156 extracts (TOEs) were dried with sodium sulfate ($NaSO_4$) and evaporated with a gentle stream of N_2 to reduce loss

157 of low-boiling compounds (cf. Ahmed and George, 2004).

158 Fifty percent of each TOE was separated over a silica gel column (0.7 g Merck silica gel 60 conditioned with *n*-

159 hexane; 1.5 cm i.d., 8 cm length) into (a) hydrocarbon (6 mL *n*-hexane), (b) alcohol (7 mL DCM/acetone, 9:1, v:v)

160 and (c) carboxylic acid fractions (DCM/MeOH, 3:1, v:v). Only the hydrocarbons were subjected to gas

161 chromatography–mass spectrometry (GC-MS).

2.5.2. Gas chromatography–mass spectrometry (GC-MS)

163 Lipid biomarker analyses of the hydrocarbon fraction were performed with a Thermo Scientific Trace 1310 GC

164 coupled to a Thermo Scientific Quantum XLS Ultra MS. The GC was equipped with a capillary column

165 (Phenomenex Zebron ZB-5MS, 30 m length, 250 µm inner diameter, 0.25 µm film thickness). Fractions were

166 injected into a splitless injector and transferred to the column at 300 °C. The carrier gas was He at a flow rate of

167 1.5 mL min^{-1}. The GC oven temperature was ramped from 80°C (1 min) to 310 °C at 5 °C min^{-1} (held for 20 min).

168 Electron ionization mass spectra were recorded in full scan mode at an electron energy of 70 eV with a mass range

169 of m/z 50 − 600 and scan time of 0.42 s. Identification of individual compounds was based on comparison of mass

170 spectra and GC retention times with published data and reference compounds.

2.5.3 Gas chromatography–combustion–isotope ratio mass spectrometer (GC-C-IRMS)

172 Compound specific δ^{13}C analyses were conducted with a Trace GC coupled to a Delta Plus IRMS via a

173 combustion-interface (all Thermo Scientific). The combustion reactor contained CuO, Ni and Pt and was operated

174 at 940°C. The GC was equipped with two serially linked capillary columns (Agilent DB-5 and DB-1; each 30 m

175 length, 250 µm inner diameter, 0.25 µm film thickness). Fractions were injected into a splitless injector and

176 transferred to the GC column at 290°C. The carrier gas was He at a flow rate of 1.2 ml min^{-1}. The temperature

177 program was identical to the one used for GC-MS (see above). CO_2 with known δ^{13}C value and a standard

178 (IAEA600) were used for internal calibration. Instrument precision was checked using a mixture of *n*-alkanes with

179 known isotopic composition. Standard deviations of duplicate sample measurements were generally better than

180 1.0 ‰. Carbon isotope ratios are expressed as δ^{13}C (‰) relative to VPDB.

2.6. Amplicon sequencing of 16S rRNA genes

2.6.1. DNA extraction and 16S rRNA gene amplification

183 Environmental DNA analyses of microbial communities were performed on a carbonate sample with embedded

184 corals from the base of the Al Gacel MV (D10-R3), a carbonate sample from an active pockmark close to the

185 summit of the Al Gacel MV (D10-R7), and a necrotic fragment of a living *Madrepora oculata* recovered from the

186 Northern Pompeia Coral Ridge (D03-B1). About 1 − 4 g of solid samples were first mashed with mortar and liquid

187 nitrogen to fine powder. Three biological replicates were used per sample. Total DNA was isolated with a Power

188 Soil DNA Extraction Kit (MO BIO Laboratories, Carlsbad, CA). All steps were performed according to the
189 manufacturer's instructions.

190 Bacterial amplicons of the V3 − V4 region were generated with the primer set MiSeq_Bacteria_V3_forward
191 primer (5'-TCGTCGGCAGCGTCAGATGTGTATAAGAGACAGCCTACGGGNGGCWGCAG-3') and
192 MiSeq_Bacteria_V4_reverse primer (5'-
193 GTCTCGTGGGCTCGGAGATGTGTATAAGAGACAGGACTACHVGGGTATCTAATCC-3'). Likewise,
194 archaeal amplicons of the V3 − V4 region were generated with the primer set MiSeq_Archaea_V3_forward primer
195 (5'-TCGTCGGCAGCGTCAGATGTGTATAAGAGACAG-GGTGBCAGCCGCCGCGGTAA-3') and
196 MiSeq_Archaea_V4_reverse primer (5'-GTCTCGTGGGCTCGGAGATGTGTATAAGAGACAG-
197 CCCGCCAATTYCTTTAAG-3'). 50 μl of the PCR reaction mixture for bacterial DNA amplification, contained
198 1 U Phusion high fidelity DNA polymerase (Biozym Scientific, Oldendorf, Germany), 5% DMSO, 0.2 mM of
199 each primer, 200 μM dNTP, 0.15 μl of 25 mM $MgCl_2$, and 25 ng of isolated DNA. The PCR protocol for bacterial
200 DNA amplification included (i) initial denaturation for 1 min at 98 °C, (ii) 25 cycles of 45 s at 98 °C, 45 s at 60 °C,
201 and 30 s at 72 °C, and (iii) a final extension at 72 °C for 5 min. The PCR reaction mixture for archaeal DNA
202 amplification was similarly prepared but contained instead 1 μl of 25 mM $MgCl_2$ and 50 ng of isolated DNA. The
203 PCR protocol for archaeal DNA amplification included (i) initial denaturation for 1 min at 98 °C, (ii) 10 cycles of
204 45 s at 98 °C, 45 s at 63 °C, and 30 s at 72 °C, (iii) 15 cycles of 45 s at 98 °C, 45 s at 53 °C, and 30 s at 72 °C, and
205 (iv) a final extension at 72 °C for 5 min.

206 PCR products were checked by agarose gel electrophoresis and purified using the GeneRead Size Selection Kit
207 (QIAGEN GmbH, Hilden, Germany).

2.6.2. Data analysis and pipeline

209 Illumina PE sequencing of the amplicons and further process of the sequence data were performed in the Göttingen
210 Genomics Laboratory (Göttingen, Germany). After Illumina MiSeq processing, sequences were analyzed as
211 described in Egelkamp et al. (2017) with minor modifications. In brief, paired-end sequences were merged using
212 PEAR v0.9.10 (Zhang et al., 2014), sequences with an average quality score below 20 and containing unresolved
213 bases were removed with QIIME 1.9.1 (Caporaso et al., 2010). Non-clipped reverse and forward primer sequences
214 were removed by employing cutadapt 1.15 (Martin, 2011). USEARCH version 9.2.64 was used following the
215 UNOISE pipeline (Edgar, 2010). In detail, reads shorter than 380 bp were removed, dereplicated, and denoised
216 with the UNOISE2 algorithm of USEARCH resulting in amplicon sequence variants (ASVs) (Callahan et al.,
217 2017). Additionally, chimeric sequences were removed using UCHIME2 in reference mode against the SILVA
218 SSU database release 132 (Yilmaz et al., 2014). Merged paired-end reads were mapped to chimera-free ASVs and
219 an abundance table was created using USEARCH. Taxonomic classification of ASVs was performed with BLAST
220 against the SILVA database 132. Extrinsic domain ASVs, chloroplasts, and unclassified ASVs were removed from
221 the dataset. Sample comparisons were performed at same surveying effort, utilizing the lowest number of
222 sequences by random subsampling (20,290 reads for bacteria, 13,900 reads for archaea).

223 The paired-end reads of the 16S rRNA gene sequencing were deposited in the National Center for Biotechnology
224 Information (NCBI) in the Sequence Read Archive SRP156750.

3. Results

3.1. The Pompeia Province — geological settings

The Pompeia Province is situated in the Gulf of Cádiz offshore Morocco, within the so-called Middle Moroccan Field (Ivanov et al., 2000) at water-depths between 860 and 1000 m (**Fig. 1**). It encompasses the active Al Gacel MV (**Fig. 1, C**), another mud volcano which is extinct (further referred as extinct MV) and two east-west elongated ridges (Northern Pompeia Coral Ridge and Southern Pompeia Coral Ridge). CWCs occur on all of these morphological features and scattered coral-mounds surround the ridges with a smooth relief (**Fig. 1, B**). Detailed geological profiles and 3D images of these features are shown in **Figs. 2** and **3**.

The Al Gacel MV is a cone-shape structure, 107 m high and 944 m wide, with its summit at 762 m depth and surrounded by a 11 m deep rimmed depression (León et al., 2012) (**Fig. 1, C**). It is directly adjacent to the Northern Pompeia Coral Ridge (**Fig. 2, A–B**), which extends ca. 4 km in westward direction (**Fig. 2, A–B**) and it is terminated by the Pompeia Escarpment (**Fig. 1, B; Fig. 2, C**). High resolution seismic profiles of the Pompeia Escarpment show CWC build-ups (R1 to R4) with steep lateral scarps of ca. 40 m height (**Fig. 2, C**). The Al Gacel MV is of sub-circular shape and exhibits a crater at its top (**Fig. 2, A–B**).

Ultra-high resolution sub-bottom seismic profile crossing the Pompeia Province from northwest (NW) to southeast (SE) (**Fig. 3, A**), shows (i) the Al Gacel MV surrounded by bottom-current deposits, (ii) an up to 130 m high CWC framework, growing on top the Southern Pompeia Coral Ridge, and (iii) semi-buried CWC mounds surrounding the ridge in areas of low relief. These CWC mounds locally form smooth, up to 25 – 30 m high topographic reliefs that are exposed, but then taper downward below the seafloor (applying sound speeds of 1750 m/s in recent sediments). Additionally, a multichannel seismic profile following the same track but with higher penetration below the seafloor (**Fig. 3, B**) shows high amplitude reflections inside the Al Gacel cone and enhanced reflections at the top of the diapirs (yellow dotted-line in **Fig. 3, B**), pointing to the occurrence of gas (hydrocarbon)-charged sediments. It furthermore exhibits breaks in seismic continuity and diapiric structures at different depths below the Southern Pompeia Coral Ridge and the Al Gacel MV, evidencing the presence of a fault system (**Fig. 3, B**). These tectonic structures may promote the development of overpressure areas (OP in **Fig. 3, B**) and consequent upward fluid flow to the surface.

3.2. ROV observation and measurements

Submersible ROV surveys at the Al Gacel MV (**Fig. 1, C**) revealed the presence of dispersed pockmark depressions at the eastern (Dive 10, 790 m) and northern flanks (Dive 11, 760 – 825 m depth). These sites are characterized by focused but low intensity seafloor bubbling (e.g. **Fig. 4, B**; **Fig. 5, A**). Analysis of water samples revealed CH_4-concentration up to 171 nM during Dive 10 and up to 192 nM during Dive 11 (Sánchez-Guillamón et al., 2015).

Pockmarks are typically characterized by grey-olive mud breccia sediments and authigenic carbonates, appearing in the center and edges. The authigenic carbonates are commonly assocaited with typical methane-seep related organisms (e.g. sulfide-oxidizing bacterial mats, chemosynthetic bivalves, siboglinid tubeworms) (**Fig. 4, B–C**; **Fig. 5**). Communities of non-chemosynthetic organisms (e.g. sponges, corals) were also found at pockmarks (**Fig. 4, B–C**; **Fig. 5, C**), but were more abundant in places where no seepage was detected (**Fig. 4, A**).

Observations with the submersible ROV at the Northern Pompeia Coral Ridge and the extinct MV (Dive 03) revealed widespread and abundant occurrences of dead scleractinian-corals (mainly *Madrepora oculata* and *Lophelia pertusa*) currently colonized by few living non-chemosynthetic organisms (e.g. *Corallium tricolor*, other

265 octocorals, sea urchins) (**Fig. 6, B–D**). Locally, grey-black colored patches of sulfide-oxidizing bacterial mats
266 surrounded by dead chemosynthetic bivalves (*Lucinoma asapheus* and *Thysira vulcolutre*) were observed (**Fig. 6,**
267 **A**). CH_4-seepage appeared to be less than at the Al Gacel MV, with concentrations of 80 – 83 nM.

268 Water parameters display homogenous values between the four sampling sites (10 °C temperature, ca. 52 – 55 %
269 dissolved oxygen, ca. 31 Kg/m^3 density) (**Table 2**). At depths of 790 m (D10-N4, same site as carbonate D10-R7)
270 and 760 m (D11-N9), the pH of seawater was 7.88 and 7.85, respectively (**Table 3**). The same seawater samples
271 exhibited ORP values of 136 mV (D10-N4) and 257 mV (D11-N9) (**Table 3**). Further analysis of these seawater
272 samples revealed Fe^{2+} concentration of 0.57 and 0.31 μM, while S^{2-} values were nearly absent (below detection
273 limit) (**Table 2**). Fe^{2+} concentrations in pore-waters ranged between 0.94 – 1.27 μM (D10-C5), 2.70 – 1.74 μM
274 (D10-C8), and 2.39 – 5.32 μM (D11-C10). S^{2-} concentrations in pore-waters were below detection limit (D10-C5),
275 50.23 μM (D10-C8), and 0.47 μM (D11-C10) (**Table 3**).

3.3. Petrography and stable isotopes signatures of carbonates ($\delta^{18}O$, $\delta^{13}C$)

277 Sample D10-R3 derives from a field of carbonates at the base of the Al Gacel MV which is inhabited by sponges
278 and corals (**Fig. 4, A**). The sample is a framestone composed of deep water scleractinian corals (*Madrepora* and
279 rare *Lophelia*) (**Fig. 7, A–B**). The corals are typically cemented by microbial automicrite (*sensu* Reitner et al.
280 1995) followed by multiple generations of aragonite. A matrix of dark allomicrite (*sensu* Reitner et al. 1995) with
281 oxidized framboidal pyrites and remains of planktonic foraminifera is restricted to few bioerosional cavities (ca.
282 5%) in the skeletons of dead corals (**Fig. 8, A–B**). $\delta^{13}C$ signatures of the matrix and cements range from −26.68 to
283 −18.38 ‰, while the embedded coral fragments exhibit $\delta^{13}C$ values between −5.58 and −2.09 ‰ (**Fig. 7, B; Table**
284 **4**). The $\delta^{18}O$ values generally range from +2.35 to +3.92 ‰ (**Fig. 9; Table 4**).

285 Sample D10-R7 was recovered from a pockmark on the eastern site of the Al Gacel MV that is virtually influenced
286 by active seepage (**Fig. 3, C**). It consists of black carbonate and exhibits a strong hydrogen sulfide (H_2S) odor (**Fig.**
287 **5, B**; **Fig. 7, C–D**). The top of this sample was inhabited by living octocorals (**Fig. 5, C**), while chemosymbiotic
288 siboglinid worms were present on the lower surface (**Fig. 5, D**). The sample is characterized by a grey peloidal
289 wackestone texture consisting of allomicrite with abundant planktonic foraminifers and few deep water miliolids.
290 The sample furthermore exhibits some fractured areas which are partly filled by granular and small fibrous cement,
291 probably consisting of Mg-calcite. Locally, light brownish crusts of microbial automicrite similar to ones in D10-
292 R3 are present (see above). Framboidal pyrite is abundant and often arranged in aggregates (**Fig. 8, C–D**). The
293 carbonate exhibits $\delta^{13}C$ values ranging from −28.77 to −21.13 ‰ and $\delta^{18}O$ values from +2.37 to +3.15 ‰ (**Fig. 9;**
294 **Table 4**).

295 Sample D11-R8 comes from an area with meter-sized carbonate blocks at the summit of the Al Gacel MV and is
296 mainly colonized by sponges and serpulid worms (**Fig. 4, D**). The sample generally exhibits a light grey mud- to
297 wackestone texture consisting of allomicrite with few scleractinian-coral fragments and planktonic foraminifers
298 (**Fig. 7, E–F**). The carbonate furthermore contains abundant quartz silt and, locally, pyrite enrichments. A further
299 prominent feature are voids that are encircled by dark grey halos and exhibit brownish margins (due to enrichments
300 of very small pyrite crystals and organic matter, respectively). $\delta^{13}C$ signatures of the matrix and cements range
301 from −14.82 to −14.74 ‰, while embedded coral fragments exhibit $\delta^{13}C$ values of −4.91 to −2.99 ‰ (**Fig. 7, F;**
302 **Table 4**). $\delta^{18}O$ values generally range from +1.49 to +5.60 ‰ (**Fig. 9; Table 4**).

303 Sample D03-B1 is a necrotic fragment of a living scleractinian coral (*Madrepora oculata*) recovered from the
304 Northern Pompeia Coral Ridge (**Fig. 6, D**; **Fig. 7, G**). The coral-carbonate exhibits $\delta^{13}C$ values ranging from -8.08
305 to -1.39 ‰ and $\delta^{18}O$ values from -0.31 to $+2.26$ ‰ (**Fig. 9**; **Table 4**).

3.4. Lipid biomarkers and compound specific carbon isotope signatures

307 The hydrocarbon fractions of the carbonate recovered from the active pockmark (D10-R7) mainly consist of the
308 irregular, tail-to-tail linked acyclic isoprenoids 2,6,11,15-tetramethylhexadecane (C_{20}; crocetane), 2,6,10,15,19-
309 pentamethylicosane (C_{25}; PMI), as well as of several unsaturated homologues of these compounds (**Fig. 10**).
310 Additionally, it contains the regular, head-to-tail linked acyclic isoprenoid pristane (C_{19}).
311 The hydrocarbon fraction of the carbonate recovered from the summit of the Al Gacel MV (D11-R8) is dominated
312 by *n*-alkanes with chain-lengths ranging from C_{14} to C_{33} (maxima at *n*-C_{16} and, subordinated, at *n*-C_{20} and *n*-C_{31})
313 (**Fig. 10**). The sample further contains pristane, a mixture of crocetane and the head-to-tail linked acyclic
314 isoprenoid phytane (C_{20}) (co-eluting), as well as traces of PMI.
315 In the carbonate from the active pockmark (D10-R7), crocetane and PMI exhibited strongly depleted $\delta^{13}C$ values
316 (-101.2 ‰ and -102.9 ‰, respectively). In the carbonate from the summit of the volcano (D11-R8),
317 crocetane/phytane and PMI showed less depleted $\delta^{13}C$ values (-57.2 ‰ and -74.3 ‰, respectively). $\delta^{13}C$ values
318 of *n*-alkanes in the carbonate D11-R8 (*n*-C_{17-22}) ranged between -30.8 ‰ and -33.0 ‰ (**Table 5**).

3.5. DNA inventories (MiSeq Illumina sequences)

320 Bacterial DNA from samples D10-R3 (authigenic carbonate, base of the Al Gacel MV) and D03-B1 (*Madrepora*
321 *oculata* fragment, Northern Pompeia Coral Ridge) mainly derives from taxa that typically thrive in the water-
322 column (e. g. Actinobacteria, Acidobacteria, Chloroflexi, Bacteroidetes, Woeseiaceae, Dadabacteria,
323 Kaiserbacteria, Poribacteria, Planctomycetes, Gemmatimonadetes) (**Fig. 11, A**). The sample D10-R3 furthermore
324 contains bacterial DNA of the nitrite-oxidizing bacteria *Nitrospira sp.*, while the sample D03-B1 contains DNA
325 of the bacterial taxa Verrucomicrobia, Enterobacteria, and *Nitrosococcus*. Noteworthy, one amplicon sequence
326 variant (ASV_189) with low number of clustered sequences has been found in D03-B1, identified as a
327 methanotrophic symbiont of *Bathymodiolus mauritanicus* (see Rodrigues et al., 2013).
328 Up to 50 % of bacterial DNA in sample D10-R7 (authigenic carbonate, top of the Al Gacel MV) derives from taxa
329 that are commonly associated with fluid seepage and AOM, i.e. sulfide-oxidizing bacteria, sulfate-reducing
330 bacteria (SRB) and methane-oxidizing bacteria. The most abundant are SRB taxa like SEEP-SRB1, SEEP-SRB2,
331 *Desulfatiglans*, *Desulfobulbus* and *Desulfococcus*, which typically form consortia with ANME archaea.
332 Archaeal DNA (**Fig. 11, B**) from samples D10-R3 and D03-B1 mainly consist of *Cenarchaeum sp.*, which
333 represents $70-90$ %. *Candidatus Nitrosopumilus* is the second most abundant in both samples, representing 5 –
334 20 %. In contrast, around 90 % of archaeal DNA in D10-R7 is related to ANME-1 and ANME-2 groups, in good
335 concordance with the relative abundances of SRB DNA.
336 Details of the number of reads per taxa are shown in the supplementary data, **Tables 1** and **2**.

4. Discussion

4.1. Evidence for hydrocarbon-rich seepage affecting the Pompeia Province

339 Two-dimensional multichannel-seismic images show that the Pompeia Province is affected by fluid expulsion
340 related to compressional diapiric ridges and thrust faults (**Fig. 3, B**), as it has been reported from other areas of the
341 Gulf of Cádiz (Somoza et al., 2003; Van Rensbergen et al., 2005; Medialdea et al., 2009). There seem to be
342 different types of fault-conduit systems that link the overpressure zones (OP) with the seafloor (**Fig. 3, B**),
343 controlling both the type and rate of seepage (e.g. eruptive, focused, diffused or intermittent, the latter referred to
344 as "dripping-like" in the following). At the Al Gacel MV, conduits are for instance mainly linked to faults and a
345 dense hydro-fracture network, allowing the migration of hydrocarbon-rich muds from the overpressure zone to the
346 surface. During active episodes, eruptions lead to the formation of mud-breccia flows as observed in gravity cores
347 (e.g. León et al., 2012). During rather dormant episodes, focused and dripping-like seepage predominates, forming
348 pockmark features (**Fig. 4, B**).

349 Currently, the Al Gacel MV is affected by continuous and focused dripping-like seepages. These sites of active
350 seepage are characterized by carbonates that are suspected to be methane-derived (e.g. sample D10-R7, **Fig. 4, B–**
351 **C**). In-situ ROV-measurements and subsequent water sample analysis demonstrated high concentrations of CH_4
352 in fluids that were escaping upon removal of the carbonate D10-R7 from the active pockmark (171 nM; **Fig. 5, A**)
353 (Sánchez-Guillamón et al., 2015). This association suggests a genetic relationship between hydrocarbon-rich
354 seepage and the carbonate, as also reflected low $\delta^{13}C$-signatures of the carbonates analyzed herein (down to ca.
355 −30 ‰, **Fig. 9; Table 3**). Indeed, the grey peloidal texture of this sample resembles that of AOM-derived
356 automicrites from the Black Sea that are related to micro-seepage of methane (cf. Reitner et al., 2005). The here
357 observed isotopically depleted acyclic isoprenoids such as crocetane and PMI ($\delta^{13}C$ values between ca. −103 and
358 −57‰; **Fig. 10; Table 4**) are typical fingerprints of AOM-associated Archaea (Hinrichs et al., 1999; Thiel et al.,
359 1999, 2001; Peckmann et al., 2001; Peckmann & Thiel, 2004), which is also in good accordance with the high
360 abundance of DNA related to ANME. At the same time, elevated concentrations of S^{2-} and Fe^{2+} in pore-waters of
361 D10-C8 micro-core (0.23 μM and 1.74 μM, respectively; **Table 2**), abundant framboidal pyrite (**Fig. 8, C–D**) and
362 SRB-related DNA in the carbonate (**Fig. 11**) evidence microbial sulfate reduction in the environment. All these
363 data clearly demonstrate that the carbonates have been formed via AOM, fueled by fluids from the underlying mud
364 diapir.

365 Other carbonate samples from the Al Gacel MV (i.e. D10-R3 and D11-R8) probably have also been formed due
366 to AOM as they are isotopically depleted as well ($\delta^{13}C$ values between ca. −25 and −15 ‰, **Fig. 9**, **Table 3**).
367 However, no active gas bubbling was observed during sampling, even though both samples still contain open voids
368 which could form pathways for fluids. Several characteristics of these voids (e.g. dark halos formed by pyrite,
369 brownish margins due to organic matter enrichments) are very similar to those of methane-derived carbonate
370 conduits (cf. Reitner et al., 2015). This could imply that the intensity of hydrocarbon-rich seepage and
371 consequently AOM, may have fluctuated through time. This in good accordance with the relatively low dominance
372 of crocetane and PMI in a carbonate sampled from the summit of Al Gacel MV (D11-R8; **Fig. 10**). The moderately
373 depleted $\delta^{13}C$ values of crocetane/phytane and PMI in this sample (−57.2 ‰ and −74.3 ‰, respectively; **Table 4**)
374 could be due to mixing effects and are thus also in agreement with varying intensities of AOM in the environment.
375 The presence of only few AOM-related DNA sequences (**Fig. 11**) and partly oxidized pyrites in the carbonate
376 D10-R3 from the base of the Al Gacel MV (**Fig. 8, A–B**) are well in line with this scenario.

377 There is no evidence for eruptive extrusions of muddy materials at the coral ridges. In the Southern Pompeia Coral
378 Ridge (**Fig. 3**), diapirs appear to rather promote an upward migration of hydrocarbon-rich fluids in a divergent
379 way throughout a more extensive seabed area. This results in a continuous and diffused seepage, which promotes

380 the occurrence of AOM and the formation of MDACs at the base of the ridges, related to the sulphate-methane

381 transition zone (SMTZ) (Boetius et al., 2000; Hinrichs and Boetius, 2002; González et al., 2012a). This is in good

382 accordance with the detection of methane (80 – 83 nM) at the Northern Pompeia Coral Ridge and the presence of

383 sulfide-oxidizing bacterial mats and shells of dead chemosynthetic bivalves at the western part of the ridge (**Fig.**

384 **6, A**). Likewise, the CWC Mounds Field surrounding the Southern Pompeia Coral Ridge (**Fig. 3**) is thoroughly

385 characterized by micro-seeps, due to ascending fluids from OPs through low-angle faults. This type of focused

386 seepage may promote formation of MDAC pavements in deeper layers of the sediments (**Fig. 3**), similar to coral

387 ridges along the Pen Duick Escarpment (Wehrmann et al., 2011). The generation of MDAC-hotspots at sites of

388 such seepage also explain the geometry of the downward tapering cones (**Fig. 3**).

389 **4.2. Ecological meaning of hydrocarbon-rich seepage for CWCs**

390 Our data suggests contemporaneous micro-seepage and CWC growth in the Pompeia Province (e.g. **Fig. 4, B**).

391 This relationship has also been observed elsewhere, e.g. in the North Sea and off Mid Norway (Hovland, 1990;

392 Hovland & Thomsen, 1997), and the Angola margin (Le Guilloux et al., 2009). Corals utilize HCO_3^- deriving from

393 both the environment and the internal production of CO_2 for skeleton biomineralization (Swart, 1983; Zoccola et

394 al., 2015; Nakamura et al., 2018). Hence, a potential utilization of methane as a carbon source should be reflected

395 in the $\delta^{13}C$ signatures of their skeletons. However, scleractinian fragments recovered from the Al Gacel MV

396 (embedded in carbonates D10-R3 and D11-R8, from the base and summit of the volcano, respectively) and the

397 Northern Pompeia Coral Ridge (D03-B1, necrotic part of a living *Madrepora oculata*) displayed barely depleted

398 $\delta^{13}C$ values (ca. −8 to −1 ‰; **Fig. 9**; **Table 3**), close to the $\delta^{13}C$ of marine seawater (0 ± 3 ‰, e.g. Hoefs, 2015).

399 These values do not support a significant uptake of methane-derived carbon by the CWCs and thus a direct trophic

400 dependency as previously proposed (Hovland, 1990). Furthermore, the only DNA in sample D03-B1 that could

401 be attributed to a potential methanotrophic endosymbiont (ASV_189: Rodrigues et al., 2013) occurred in minor

402 amounts and most likely represents contamination from the environment or during sampling. It appears therefore

403 more likely that the CWCs feed on a mixture of phytoplankton, zooplankton and dissolved organic matter as

404 previously proposed for ones in other regions (Kiriakoulakis et al., 2005; Duineveld et al., 2007; Becker et al.,

405 2009; Liebetrau et al., 2010). This is in good accordance with the presence of DNA from various common archaeal

406 and bacterial taxa (e.g. Acidobacteria, Actinobacteria, Candidatus *Nitrosopumilus*, *Cenarchaeum sp.*) and some

407 potential members of the corals' holobiont (e.g. Enterobacteria, Verrucomicrobia, *Nitrosococcus sp.*) (Sorokin,

408 1995; Rädecker et al., 2015; Webster et al., 2016) in sample D03-B1 (**Fig. 11**). Taken together, there is no evidence

409 that CWCs in the working area harbor microbial symbionts which potentially could utilize the hydrocarbon-rich

410 fluids. However, future analyses on living coral-tissue will be important to verify this conclusion.

411 CWC development and hydrocarbon-rich seepage appear to be rather linked *via* the formation of MDAC deposits,

412 which provide the hard substrata needed for CWC larval settlement (e.g. Díaz-del-Rio et al., 2003; Van Rooij et

413 al., 2011; Magalhães et al., 2012; Le Bris et al., 2016; Rueda et al., 2016). If too severe, however, fluid flow and

414 associated metabolic processes can result in local conditions that are lethal to CWCs (see 4.3). Moreover, AOM

415 fueled by fluid flow can also cause an entombment of the CWCs by MDACs (Wienberg et al., 2009, Wienberg &

416 Titschack, 2015), as observed in D10-R3 and D11-R8 carbonates from the Al Gacel MV (**Figs. 7 and 9**; **Tables 3**

417 **and 4**). It is therefore not surprising that large CWC systems in the Pompeia Province are always linked to

418 structures that are affected by rather mild, non-eruptive seepage (i.e. the extinct MV, the coral ridges and the CWC

419 Mound Fields: **Figs. 3 and 6**). The observation that these systems are in large parts "coral graveyards" (**Fig. 6, B–**

D), similar to other areas in the Gulf of Cádiz (see Foubert et al., 2008; Wienberg et al., 2009), may be explained by a post-glacial decrease in current strength (Foubert et al., 2008). In the light of our findings, however, they could also have been negatively affected by periods of intensive seepage during higher tectonic activity. Future studies are important to test this hypothesis in greater detail.

4.3. Spatio-temporal co-existence of CWCs and chemosynthetic organisms — the buffer effect

As discussed above, MDAC deposits are ecologically beneficial for CWCs, as they serve as optimal substrata even when seepage is still present (e. g. Hovland, 1990; Hovland & Thomsen, 1997; Le Guilloux et al., 2009; this study). Severe hydrocarbon-rich seepage, however, is ecologically stressful for the corals. Particularly, fluid- and AOM-derived hydrogen sulfide is considered problematic because of its role in coral necrosis (Myers & Richardson, 2009; García et al., 2016) and carbonate dissolution effects (Wehrmann et al., 2011).

Hydrogen sulfides can efficiently be buffered through the reaction with Fe-(oxyhydro)-oxides or Fe^{2+} dissolved in pore waters, ultimately forming pyrite (Wehrmann et al., 2011). Fe-(oxyhydro)-oxides nodules have previously been observed in the Iberian and Moroccan margins (González et al., 2009; 2012b), but not in the Pompeia Province. Instead, sulfide-oxidizing bacteria living in symbiosis with invertebrates (e.g. siboglinid worms: Petersen & Dubilier, 2009) (**Fig. 5, D**) and thriving in mats (**Fig. 4, C**; **Fig. 6, A**) were particularly prominent along this region. These microbes may form a biological buffer by withdrawing reduced sulfur species through their metabolic activity. Likewise, the consumption of methane and sulfate by AOM-microorganisms at active sites also contribute to CWCs colonization of the carbonates by reducing environmental acidification (seawater pH was 7.85 in the active pockmark from the Al Gacel MV; see section 3.2).

We propose that this biological buffer provides a further ecological linkage between hydrocarbon-rich seepage and cold-water corals along the Pompeia Province ("buffer effect model": **Fig. 12**). This model explains the observed co-existence of non-chemosynthetic corals (e.g. on top of D10-R7 carbonate: **Fig. 5**) with AOM-microorganisms and chemosynthetic sulfide-oxidizing organisms at pockmark sites at the Al Gacel MV (**Fig. 12, A**). At the same time, it is in line with associations of sulfide-oxidizing bacterial mats, scleractinian corals, and other non-chemosynthetic octocorals at diapiric ridges and coral mounds in the Northern Pompeia Coral Ridge (**Fig. 12, B, C**). The impact and exact capacity of this biological buffer, however, remains elusive and must be evaluated in future studies.

5. Conclusions

Cold-water coral occurrences in the Pompeia Province (Gulf of Cádiz) are typically linked to hydrocarbon-seep structures like mud volcanoes and diapirs. The irregular topography of these structures affects bottom water-currents which supply nutrients to the corals. A further ecological benefit is the seepage-fueled formation of authigenic carbonates, which provide ideal substrates for coral larvae settlement. Cold-water corals therefore take indirectly advantages of seepage-related conditions, instead of feeding from the seeped fluids, such as sulfide and methane. However, increased fluid seepage appears to be ecologically disadvantageous as evidenced by corals embedded in some of the carbonates. Consequently, cold-water coral growth in these habitats depends directly on seepage intensity and how these fluids are drained onto the seafloor (i.e. eruptive, focused, diffused or dripping-like). Cold-water coral growth appears to be furthermore supported by the microbial-mediated removal of seepage-related toxic substances (e. g., reduced sulfur species through sulfide-oxidizing bacteria) and shaping of

458 environmental conditions (e. g., pH-buffering through AOM). This biological buffer is possibly crucial to keep
459 conditions favorable for the growth of cold-water corals in the studied area, particularly in times of increased fluid
460 seepage.

Author contribution

462 Blanca Rincón-Tomás, Dominik Schneider and Michael Hoppert carried out the microbial analysis. Jan-Peter
463 Duda carried out the biomarker analysis. Luis Somoza and Teresa Medialdea processed seismic and bathymetric
464 data. Pedro Madureira processed ROV data. Javier González and Joachim Reitner carried out the petrographic
465 analysis. Esther Santofimia and Enrique López-Pamo carried out the pore-water and seawater analysis. Joachim
466 Reitner carried out the stable isotopic analysis. Blanca Rincón-Tomás prepared the manuscript with
467 contributions from all co-authors.

Competing interests

469 The authors declare that they have no conflict of interest.

References

477 Ahmed, M. and George, S.C.: Changes in the molecular composition of crude oils during their preparation for GC
478   and GC–MS analyses, Org. Geochem., 35, 137–155, doi:10.1016/j.orggeochem.2003.10.002, 2004.
479 Becker, E. L., Cordes, E. E., Macko, S. A., and Fisher, C. R.: Importance of seep primary production to *Lophelia*
480   *pertusa* and associated fauna in the Gulf of Mexico, Deep-sea Res Pt I, 56(5), 786–800,
481   doi:10.1016/j.dsr.2008.12.006, 2009.
482 Birgel, D., Thiel, V., Hinrichs, K. U., Elvert, M., Campbell, K. A., Reitner, J., Farmer, J. D., and Peckmann, J.:
483   Lipid biomarker patterns of methane-seep microbialites from the Mesozoic convergent margin of
484   California, Org. Geochem., 37(10), 1289–1302, doi:10.1016/j.orggeochem.2006.02.004, 2006.
485 Boetius, A., Ravenschlag, K., Schubert, C. J., Rickert, D., Widdel, F., Gieseke, A., Amann, R., Jørgensen, B. B.,
486   Witte, U., and Pfannkuche, O.: A marine microbial consortium apparently mediating anaerobic oxidation
487   of methane, Nature, 407 (6804), 623–626, doi:10.1038/35036572, 2000.
488 Callahan, B., MacMurdie, P. J., and Holmes, S. O.: Exact sequence variants should replace optional taxonomic
489   units in marker-gene data analysis, ISME J., 11, 2639–2643, doi:10.1038/ismej.2017.119, 2017.
490 Caporaso, J.G., Kuczynski, J., Stombaugh, J., Bittinger, K., Bushman, F.D., Costello, E.K., Fierer, N., González-
491   Peña, A., Goodrich, J. K., Gordon, J. I., Huttley, G. A., Knights, D., Koenig, J. E., Lozupone, C. A.,
492   McDonald, D., Muegge, B. D., Pirrung, M., Reeder, J., Sevinsky, J. R., Turnbaugh, P. J., Walters, W. A.,

Widmann, J., Yatsunenko, T., Zaneveld, J., and Knight, R.: QIIME allows analysis of high-throughput community sequencing data, Nat. Methods, 7, 335–336, doi:10.1038/nmeth.f.303, 2010.

Cordes, E., Arnaud-Haond, S., Bergstad, O., da Costa Falcão, A. P., Freiwald, A., Roberts, J. M., and Bernal, P.: Cold water corals, in: The First Global Integrated Marine Assessment, World Ocean Assessment I, United Nations, Cambridge University Press, Cambridge, United Kingdom, 2016.

Díaz-del-Río, V., Somoza, L., Martínez-Frías, J., Mata, M. P., Delgado, A., Hernandez-Molina, F. J., …, Vázquez, J. T.: Vast fields of hydrocarbon-derived carbonate chimneys related to the accretionary wedge/olistostrome of the Gulf of Cádiz, Mar. Geol., 195, 177–200, doi:10.1016/S0025-3227(02)00687-4, 2003.

Dorschel, B., Hebbeln, D., Foubert, A., White, M., and Wheeler, A. J.: Hydrodynamics and cold-water coral facies distribution related to recent sedimentary processes at Galway Mound west of Ireland, Mar. Geol., 244, 184–195, doi:10.1016/j.margeo.2007.06.010, 2007.

Duineveld, G. C., Lavaleye, M. S., Bergman, M. J., De Stigter, H., and Mienis, F.: Trophic structure of a cold-water coral mound community (Rockall Bank, NE Atlantic) in relation to the near-bottom particle supply and current regime, B. Mar. Sci., 81 (3), 449–467, 2007.

Dullo, W. C., Flögel, S., and Rüggerberg, A.: Cold-water coral growth in relation to the hydrography of the Celtic and Nordic European continental margin, Mar. Ecol. Prog. Ser., 371, 165–176, doi:10.3354/meps07623, 2008.

Dunham, R. J., 1962, Classification of carbonate rocks according to their depositional texture, in: Classification of Carbonate Rocks, Ham, W. E. (Eds.), American Association of Petroleum Geologists Memoir 1, Tulsa, OK, 108–121, 1962.

Edgar, R. C.: USEARCH. http://www.drive5.com/usearch. 2010.

Egelkamp, R., Schneider, D., Hertel, R., and, Daniel, R.: Nitrile-Degrading Bacteria Isolated from Compost, Front. Environ. Sci., 5, doi: 10.3389/fenvs.2017.00056, 2017.

Embry III, A. F., and Klovan, J. E.: A late Devonian reef tract on northeastern Banks Island, NWT, B. Can. Petrol. Geol., 19(4), 730–781, 1971.

Foubert, A., Depreiter, D., Beck, T., Maignien, L., Pannemans, B., Frank. N., Blamart, D., and Henriet, J.: Carbonate mounds in a mud volcano province off north-west Morocco: key to processes and controls, Mar. Geol., 248, 74–96, doi: 10.1016/j.margeo.2007.10.012, 2008.

Garcia, G. D., Santos, E. D. O., Sousa, G. V., Zingali, R. B., Thompson, C. C., and Thompson, F. L.: Metaproteomics reveals metabolic transitions between healthy and diseased stony coral *Mussismilia braziliensis*, Mol. Ecol., 25(18), 4632–4644, doi:10.1111/mec.13775, 2016.

Goedert, J. L., and Peckmann, J.: Corals from deep-water methane-seep deposits in Paleogene strata of Western Oregon and Washington, U.S.A., in: Cold-water corals and Ecosystems, Freiwald, A., and Roberts, J. M. (eds.), Springer-Verlag, Berlin Heidelberg, 27–40, 2005.

Gomes-Sumida, P.Y., Yoshinaga, M.Y., Saint-Pastous Madureira, L.A., and Hovland, M.: Seabed pockmarks associated with deep water corals off SE Brazilian continental slope, Santos Basin, Mar. Geol., 207, 159–167, doi:10.1016/j.margeo.2004.03.006, 2004.

González, F. J., Somoza, L., Lunar, R., Martínez-Frías, J., Martín Rubí, J. A., Torres, T., Ortiz, J. E., Díaz-del-Río, V., Pinheiro, L. M., and Magalhães, V. H.: Hydrocarbon-derived ferromanganese nodules in

533   carbonate mud mounds from the Gulf of Cádiz: mud-breccia sediments and clasts as nucleation sites,

534   Mar. Geol., 261, 64–81, doi:10.1016/j.margeo.2008.11.005, 2009.

535 González, F. J., Somoza, L., León, R., Medialdea, T., de Torres, T., Ortiz, J. E., Martínez-Frías, J., and Merinero,

536   R.: Ferromanganese nodules and micro-hardgrounds associated with the Cádiz Contourite Channel (NE

537   Atlantic): Palaeoenvironmental records of fluid venting and bottom currents, Chem. Geol., 310–311, 56–

538   78, doi: 10.1016/j.chemgeo.2012.03.030, 2012a.

539 González, F. J., Somoza, L., Medialdea, T., León, R., Torres, T., Ortiz, J. E., and Martín-Rubí, J. A.: Discovery of

540   ferromanganese hydrocarbon-related nodules associated with the Meknes mud volcano (Western

541   Moroccan margin). European Geoscience Union 2012 (EGU2012). Viena (Austria). Geophys. Res. Abs.

542   vol. 14, EGU2012-12306, 2012b.

543 Hebbeln, D., Van Rooij, D., and Wienberg, C.: Good neighbours shaped by vigorous currents: cold-water coral

544   mounds and contourites in the North Atlantic, Mar. Geol, 378, 171–185,

545   doi:10.1016/j.margeo.2016.01.014, 2016.

546 Hensen, C., Nuzzo, M., Hornibrook, E., Pinheiro, L.M., Bock, B., Magalhães, V.H., and Brückmann, W.: Sources

547   of mud volcano fluids in the Gulf of Cádiz — indications for hydrothermal imprint, Geochim.

548   Cosmochim. Ac., 71 (5), 1232–1248, doi:10.1016/j.gca.2006.11.022, 2007.

549 Hinrichs, K. -U., and Boetius, A.: The anaerobic oxidation of methane: new insights in microbial ecology and

550   biogeochemistry, in: Ocean Margin Systems, Wefer, G., Billett, D., Hebbeln, D., Jørgensen, B.B.,

551   Schlueter, M., Van Weering, T. (Eds.), Springer-Verlag, Berlin, 457–477, 2002.

552 Hinrichs, K. -U., Hayes, J. M., Sylva, S. P., Brewer, P. G., and De Long, E. F.: Methane-consuming archaebacteria

553   in marine sediments, Nature, 398, 802–805, doi:10.1038/19751, 1999.

554 Hoefs, J.: Stable Isotope Geochemistry, Springer, Berlin, 2015.

555 Hovland, M.: Do carbonate reefs form due to fluid seepage?, Terra Nova, 2, 8–18, doi:10.1111/j.1365-

556   3121.1990.tb00031.x, 1990.

557 Hovland, M., Jensen, S., and Indreien, T.: Unit pockmarks associated with *Lophelia* coral reefs off mid-Norway:

558   more evidence of control by 'fertilizing' bottom currents, Geo-Mar. Lett., 32 (5–6), 545–554,

559   doi:10.1007/s00367-012-0284-0, 2012.

560 Hovland, M., Mortensen, P. B., Brattegard, T., Strass, P., and Rokoengen, K.: Ahermatypic coral banks off mid-

561   Norway: evidence for a link with seepage of light hydrocarbons, Palaios, 13, 189–200, doi:10.1043/0883-

562   1351(1998)013<0189:ACBOME>2.0.CO;2, 1998.

563 Hovland, M., and Thomsen, E.: Cold-water corals — are they hydrocarbon seep related?, Mar. Geol., 137, 159–

564   164, doi:10.1016/S0025-3227(96)00086-2, 1997.

565 Huvenne, V. A., Masson, D. G., and Wheeler, A. J.: Sediment dynamics of a sandy contourite: the sedimentary

566   context of the Darwin cold-water coral mounds, Northern Rockall Trough, Int. J. Earth Sci., 98 (4), 865–

567   884, doi: 10.1007/s00531-008-0312-5, 2009.

568 Ivanov, M. K., Akhmetzhanov, A. M., and Akhmanov, G. G.: Multidisciplinary study of geological processes on

569   the North East Atlantic and Western Mediterranean Margins, in: Ioc. Tech. S., 56, UNESCO, 2000.

570 Kiriakoulakis, K., Fisher, E., Wolff, G. A., Freiwald, A., Grehan, A., and Roberts, J. M.: Lipids and nitrogen

571   isotopes of two deep-water corals from the North-East Atlantic: initial results and implications for their

572   nutrition, in: Cold-Water Corals and Ecosystems, Freiwald, A., Roberts, J. M. (Eds.), Erlangen Earth

573   Conf., Springer, Germany, 715–729, 2005.

Le Bris, N., Arnaud-Haond, S., Beaulieu, S., Cordes, E. E., Hilario, A., Rogers, A., van de Gaever, S., and Watanabe, H.: Hydrothermal Vents and Cold Seeps, in: The First Global Integrated Marine Assessment, United Nations, Cambridge University Press, Cambridge, United Kingdom, 2016.

Le Guilloux, E., Olu, K., Bourillet, J. F., Savoye, B., Iglésias, S. P., and Sibuet, M.: First observations of deep-sea coral reefs along the Angola margin, Deep-sea Res. Pt. II, 56, 2394–2403, doi:10.1016/j.dsr2.2009.04.014, 2009.

Liebetrau, V., Eisenhauer, A., and Linke, P.: Cold seep carbonates and associated cold-water corals at the Hikurangi Margin, New Zealand: new insights into fluid pathways, growth structures and geochronology, Mar. Geol., 272, 307–318, doi:10.1016/j.margeo.2010.01.003, 2010.

León, R., Somoza, L., Medialdea, T., Vázquez, J. T., González, F. J., López-González, N., Casas, D., del Pilar Mata, M., del Fernández-Puga, C., Giménez-Moreno, C. J., and Díaz-del-Río, V.: New discoveries of mud volcanoes on the Moroccan Atlantic continental margin (Gulf of Cádiz): morpho-structural characterization, Geo-Mar. Lett., 32, 473–488, doi:10.1007/s00367-012-0275-1, 2012.

Magalhães, V. H., Pinheiro, L. M., Ivanov, M. K., Kozlova, E., Blinova, V., Kolganova, J., Vasconcelos, C., McKenzie, J. A., Bernasconi, S. M., Kopf, A., Díaz-del-Río, V., González, F. J., and Somoza, L.: Formation processes of methane-derived authigenic carbonates from the Gulf of Cádiz, Sediment. Geol., 243–244, 155–168, doi:10.1016/j.sedgeo.2011.10.013, 2012.

Margreth, S., Gennari, G., Rüggeberg, A., Comas, M. C., Pinheiro, L. M., and Spezzferri, S.: Growth and demise of cold-water coral ecosystems on mud volcanoes in the West Alboran Sea: The messages from planktonic and benthic foraminifera, Mar. Geol., 282, 26–39, doi:10.1016/j.margeo.2011.02.006, 2011.

Martin, M.: Cutadapt removes Adapter Sequences from High-Throughput Sequencing Reads, EMBnet.jounal, 10–12, doi: 10.14806/ej.17.1.200, 2011.

Medialdea, T., Somoza, L., Pinheiro, L. M., Fernández-Puga, M. C., Vázquez, J. T., León, R., Ivanov, M. K., Magalhães, V., Díaz-del-Río, V., and Vegas, R.: Tectonics and mud volcano development in the Gulf of Cádiz, Mar. Geol., 261, 48–63, doi:10.1016/j.margeo.2008.10.007, 2009.

Mortensen, P. B., Hovland, M. T., Fossa, J. H., and Furevik, D. M.: Distribution, abundance and size of *Lophelia pertusa* coral reefs in mid Norway in relation to seabed characteristics, J. Mar. Biol. Assoc. UK, 81, 581–597, doi:10.1017/S002531540100426X, 2001.

Myers, J.L., and Richardson, L.L.: Adaptation of cyanobacteria to the sulfide-rich microenvironment of black band disease of coral, FEMS Microbiol. Ecol., 67, 242–251, doi:10.1111/j.1574-6941.2008.00619.x, 2009.

Nakamura, T., Nadaoka, K., Watanabe, A., Yamamoto, T., Miyajima, T., and Blanco, A. C.: Reef-scale modeling of coral calcification responses to ocean acidification and sea-level rise, Coral Reefs, 37, 2018.

Peckmann, J., Reimer, A., Luth, U., Luth, C., Hansen, B.T., Heinicke, C., Hoefs, J., and Reitner, J.: Methane-derived carbonates and authigenic pyrite from the northwestern Black Sea, Mar. Geol., 177, 129–150, doi:10.1016/S0025-3227(01)00128-1, 2001.

Peckmann, J., and Thiel, V.: Carbon cycling at ancient methane–seeps, Chem. Geol., 205 (3), 443–467, doi:10.1016/j.chemgeo.2003.12.025, 2004.

Petersen, J. M., and Dubilier, N.: Methanotrophic symbioses in marine invertebrates, Env. Microbiol. Rep., 1(5), 319–335, doi:10.1111/j.1758-2229.2009.00081.x, 2009.

613 Pinheiro, L. M., Ivanov, M. K., Sautkin, A., Akhmanov, G., Magalhães, V. H., Volkonskaya, A., Monteiro, J. H.,
614   Somoza, L., Gardner, J., Hamouni, N., and Cunha, M. R.: Mud volcanism in the Gulf of Cádiz: results
615   from the TTR-10 cruise, Mar. Geol., 195, 131–151, doi:10.1016/S0025-3227(02)00685-0, 2003.

616 Rädecker, N., Pogoreutz, C., Voolstra, C. R., Wiedenmann, J., and Wild, C.: Nitrogen cycling in corals: The key
617   to understanding holobiont functioning?, Trends Microbiol., 23 (8), 490–497,
618   doi:10.1016/j.tim.2015.03.008, 2015.

619 Reitner, J., Gauret, P., Marin, F., and Neuweiler, F.: Automicrites in a modern marine microbialite. Formation
620   model via organic martices (Lizard Island, Great Barrier Reef, Australia), Bull.-Inst. Oceanogr. Monaco,
621   14, 237–263, 1995.

622 Reitner, J., Blumenberg, M., Walliser, E. -O., Schäfer, N., and Duda, J. -P.: Methane-derived carbonate conduits
623   from the late Aptian of Salinac (Marne Bleues, Vocontian Basin, France): Petrology and biosignatures,
624   Mar. Petrol. Geol., 66 (3), 641–652, doi:10.1016/j.marpetgeo.2015.05.029, 2015.

625 Reitner, J., Peckmann, J., Blumenberg, M., Michaelis, W., Reimer, A., and Thiel, V.: Concretionary methane-seep
626   carbonates and associated microbial communities in Black Sea sediments, Palaeogeogr., Palaeoclimatol.,
627   Palaeocl., 227, 18–30, doi:10.1016/j.palaeo.2005.04.033, 2005.

628 Roberts, J. M., Long, D., Wilson, J. B., Mortensen, P. B., and Gage, J. D.: The cold-water coral *Lophelia pertusa*
629   (Scleractinia) and enigmatic seabed mounds along the north-east Atlantic margin: are they related?, Mar.
630   Pollut. Bull., 46, 7–20, doi:10.1016/S0025-326X(02)00259-X, 2003.

631 Roberts, J. M., Wheeler, A. J., and Freiwald, A.: Reefs of the deep: the biology and geology of cold-water coral
632   ecosystems, Science, 312 (5773), 543–547, doi:10.1126/science.1119861, 2006.

633 Roberts, J. M., Wheeler, A., Freiwald, A., and Cairns, S. (Eds.): Cold-water corals: the biology and geology of
634   deep-sea coral habitats, Cambridge University Press, Cambridge, United Kingdom, 2009.

635 Rodrigues, C. F., Cunha, M. R., Génio, L., and Duperron, S.: A complex picture of associations between two host
636   mussels and symbiotic bacteria in the Northeast Atlantic, Naturwissenschaften, 100, 21–31,
637   doi:10.1007/s00114-012-0985-2, 2013.

638 Rogers, A. D.: The Biology of *Lophelia pertusa* (Linnaeus 1758) and other Deep-Water Reef-Forming Corals and
639   Impacts from Human Activities, Int. Rev. Hydrobiol., 84 (4), 315–406, doi:10.1002/iroh.199900032,
640   1999.

641 Rueda, J. L., González-García, E., Krutzky, C., López-Rodríguez, J., Bruque, G., López-González, N., Palomino,
642   D., Sánchez, R. F., Vázquez, J. T., Fernández-Salas, L. M., and Díaz-del-Río, V.: From chemosynthetic-
643   based communities to cold-water corals: Vulnerable deep-sea habitats of the Gulf of Cádiz, Mar.
644   Biodiver., 46, 473–482, doi:10.1007/s12526-015-0366-0, 2016.

645 Sánchez-Guillamón, O., García, M. C., Moya-Ruiz, F., Vázquez, J. T., Palomino, D., Fernández-Puga, M. C., and
646   Sierra, A.: A preliminary characterization of greenhouse gas (CH_4 and CO_2) emissions from Gulf of Cádiz
647   mud volcanoes, VIII Symposium MIA15, 2015.

648 Somoza, L., Ercilla, G., Urgorri, V., León, R., Medialdea, T., Paredes, M., González, F. J., and Nombela, M. A.:
649   Detection and mapping of cold-water coral mounds and living *Lophelia* reefs in the Galicia Bank, Atlantic
650   NW Iberia margin, Mar. Geol., 349, 73–90, doi:10.1016/j.margeo.2013.12.017, 2014.

651 Somoza, L., León, R., Ivanov, M. Fernández-Puga, M. C., Gardner, J. M., Hernández-Molina, F. J., Pinheiro, L.
652   M., Rodero, J., Lobato, A., Maestro, A., Vázquez, J. T., Medialdea, T., and Fernández-Salas, L. M.:
653   Seabed morphology and hydrocarbon seepage in the Gulf of Cádiz mud volcano area: Acoustic imagery,

multibeam and ultra-high resolution seismic data, Mar. Geol., 195, 153–176, doi:10.1016/S0025-3227(02)00686-2, 2003.

Sorokin, Y. I.: Coral reef ecology, Springer, Germany, 1995.

Suess, E, and Whiticar, M. J.: Methane-derived CO_2 in pore fluids expelled from the Oregon subduction zone, Palaeogeogr., Palaeoclimatol., Palaeocl., 71, 119–136, doi:10.1016/0031-0182(89)90033-3, 1989.

Swart, P. K.: Carbon and Oxygen Isotope Fractionation in ScleracUnian Corals: a Review, Earth-Sci. Rev., 19, 51–80, 1983.

Thiel, V., Peckmann, J., Seifert, R.,Wehrung, P., Reitner, J., and Michaelis, W.: Highly isotopically depleted isoprenoids: molecular markers for ancient methane venting, Geochim. Cosmochim. Ac., 63, 3959–3966, doi:10.1016/S0016-7037(99)00177-5, 1999.

Thiel, V., Peckmann, J., Richnow, H.-H., Luth, U., Reitner, J., and Michaelis, W.: Molecular signals for anaerobic methane oxidation in Black Sea seep carbonates and a microbial mat, Mar. Chem. 73, 97–112, doi:10.1016/S0304-4203(00)00099-2, 2001.

Thiem, Ø., Ravagnan, E., Fosså, J. H., and Berntsen, J.: Food supply mechanisms for cold- water corals along a continental shelf edge, J. Marine Syst., 26, 1481–1495, doi:10.1016/j.jmarsys.2005.12.004, 2006.

Vandorpe, T., Martins, I., Vitorino, J., Hebbeln, D., García-García, M., and Van Rooij, D.: Bottom currents and their influence on the sedimentation pattern in the El Arraiche mud volcano province, southern Gulf of Cádiz, Mar. Geol., 378, 114–126, doi:10.1016/j.margeo.2015.11.012, 2016.

Vandorpe, T., Wienberg, C., Hebbeln, D., Van den Berghe, M., Gaide, S., Wintersteller, P., and Van Rooij, D.: Multiple generations of buried cold-water coral mounds since the Early-Middle Pleistocene Transition in the Atlantic Moroccan Coral Province, southern Gulf of Cádiz, Palaeogeogr., Palaeoclimatol., Palaeocl., 485, 293–304, doi:10.1016/j.palaeo.2017.06.021, 2017.

Van Rensbergen, P., Depreiter, D., Pannemans, B., Moerkerke, G., Van Rooij, D., Marsset, B., Akhmanov, G., Blinova, V., Ivanov, M., Rachidi, M., Magalhães, V., Pinheiro, L., Cunha, M., and Henriet, J.P.: The Arraiche mud volcano field at the Moroccan Atlantic slope, Gulf of Cádiz, Mar. Geol., 219, 1–17, doi:10.1016/j.margeo.2005.04.007, 2005.

Van Rooij, D., Blamart, D., De Mol, L., Mienis, F., Pirlet, H., Whermann, L. M., …, Henriet, J. -P.: Cold-water coral mounds on the Pen Duick Escarpment, Gulf of Cádiz: The MiCROSYSTEMS project approach, Mar. Geol., 282, 102–117, doi:10.1016/j.margeo.2010.08.012, 2011.

Watling, L., France, S. C., Pante, E., and Simpson, A.: Biology of Deep-Water Octocorals, in: Advances in Marine Biology Volume 60, Lesser, M. (Eds.), Academic Press, London, United Kingdom, 41–122, 2011.

Webster, N. S., Negri, A. P., Botté, E. S., Laffy, P. W., Flores, F., Noonan, S., Schmidt, C., and Uthicke, S.: Host-associated coral reef microbes respond to the cumulative pressures of ocean warming and ocean acidification Sci. Rep.-UK, 6, doi:10.1038/srep19324, 2016.

Wheeler, A. J., Beyer, A., Freiwald, A., de Haas, H., Huvenne, V. A., Kozachenko, M., Olu-Le Roy, K., and Opderbecke, J.: Morphology and environment of cold-water coral carbonate mounds on the NW European margin, Int. J. Earth Sci., 96, 37–56, doi:10.1007/s00531-006-0130-6, 2007.

Wehrmann, L. M. Templer, S. P., Brunner, B., Bernasconi, S. M., Maignien, L., and Ferdelman, T. G.: The imprint of methane seepage on the geochemical record an early diagenetic processes in cold-water coral mounds on Pen Duick Escarpment, Gulf of Cádiz, Mar. Geol., 118–137, doi:10.1016/j.margeo.2010.08.005, 2011.

694   Wienberg, C., Hebbeln, D., Fink, H. G., Mienis, F., Dorschel, B., Vertino, A., López-Correa, M., and Freiwald,
695   A.: Scleractinian cold-water corals in the Gulf of Cádiz—first clues about their spatial and temporal
696   distribution, Deep-sea Res. Pt. I, 56 (10), 1873–1893, doi:10.1016/j.dsr.2009.05.016, 2009.

697   Wienberg, C., and Titschack, J.: Framework-forming scleractinian cold-water corals through space and time: a
698   late Quaternary North Atlantic perspective, in: Marine Animal Forests: The Ecology of Benthic
699   Biodiversity Hotspots, Rossi, S., Bramanti, L., Gori, A., and Orejas, C. (Eds.), Springer, Cham,
700   Switzerland, 1–34, 2015.

701   Yilmaz, P., Parfrey, L.W., Yarza, P., Gerken, J., Pruese, E., Quast, C., Schweer, T., Peplies, J., Ludwig, W., and
702   Glöckner, F. O.: The SILVA and 'All-species Living Tree Project (LTP)' taxonomic frameworks, Nucleic
703   Acids Res., 42, D643–D648, doi:10.1093/nar/gkt1209, 2014.

704   Zhang, J., Kobert, K., Flouri, T., and Stamatakis, A.: PEAR: a fast and accurate Illumina Paired-End reAd
705   merger, Bioinformatics, 30 (5), 614–620, doi:10.1093/bioinformatics/btt593, 2014.

706   Zoccola, D. Ganot, P., Bertucci, A., Caminit-Segonds, N., Techer, N., Voolstra, C. R., Aranda, M., Tambutté, E.,
707   Allemand, D., Casey, J. R., and Tambutté, S.: Bicarbonate transporters in corals point towards a key step
708   in the evolution of cnidarian calcification, Sci. rep.-UK, 5, 2015.

709

710

711

712

713

714

715

716

717

718

719

720

721

722

723

724

725

726

727

728

729 **Table 1**. General description and characterization of recovered samples for this study in the Al Gacel MV and
730 Northern Pompeia Province.

	Site description	Coordinates	Depth (m)	Type	Sample
Al Gacel MV	Base of volcano characterized by non-chemosynthetic fauna	35° 26.51' N 6° 58.22' W	850 – 890	Carbonate	D10-R3
	Active pockmark	35° 26.47' N 6° 58.27' W	790	Carbonate	D10-R7
				Water	D10-N4
					D10-C5
					D10-C8
	Summit with metric carbonate blocks	35° 26.48' N 6° 58.35' W	763	Carbonate	D11-R8
		35° 26.48' N 6° 58.37' W	760	Water	D11-N9
					D11-C10
Northern Pompeia Coral Ridge	Sulfide-oxidizing bacterial mats and shells of chemosynthetic bivalves	35° 26.77' N 6° 59.94' W	829	Necrotic fragment of a living *Madrepora oculata* coral	D03-B1

731

732 **Table 2.** *In-situ* water variables measured during sampling with ROV sensors.

	D10-R3	D10-R7	D11-R8	D03-B1
Temperature (°C)	10.07	10.5	10.02	10.04 – 10.05
Conductivity (mS/cm)	39.13 – 39.62	39.05 – 39.43	-	-
Salinity (ppt)	-	-	35.56 – 35.86	35.67 – 35.91
Saturation of dissolved oxygen (%)	53.64 – 54.69	54.02 – 54.35	51.95 – 53.92	52.46 – 56.22
Dissolved oxygen (mg/l)	4.81 – 4.90	4.85 – 4.88	4.66 – 4.84	4.71 – 5.09
Density (kg/m^3)	31.03 – 31.42	30.94 – 31.24	30.92 – 31.08	31.26 – 31.41

733

734 **Table 3**. On site measurements of soluble Fe^{2+} and S^{2+} values from seawater and pore-water. Please note that

735 samples D10-C5, D10-C8 and D10-N4 were taken from the same site as the authigenic carbonate D10-R7 (see

736 **Fig. 2**). d.l. = detection limit.

Sample	Type	Fe^{2+} (μM)	S^{2+} (μM)	pH	ORP (mV)
D10-C5 (0 – 6 cm)	Pore-water	0.94	< d.l.	-	-
D10-C5 (6 –16 cm)		1.27	< d.l.	-	-
D10-C8 (0 – 6 cm)		2.70	< d.l.	-	-
D10-C8 (6 –16 cm)		1.74	0.23	-	-
D10-N4	Sea-water	0.57	< d.l.	7.88	136
D11-C10 (0 – 5 cm)	Pore-water	2.39	< d.l.	-	-
D11-C10 (5 – 15 cm)		5.32	0.47	-	-
D11-N9	Seawater	0.31	< d.l.	7.85	257

737
738
739
740
741
742
743
744
745
746
747
748
749
750
751
752
753
754
755

756   **Table 4.** Stable carbon and oxygen isotopes ($\delta^{13}C$, $\delta^{18}O$) of samples from the Al Gacel MV and the Northern

757   Pompeia Coral Ridge.

Location	Sample	Origin of the carbonate	Identification number in Fig. 7	$\delta^{18}O$ (‰)	$\delta^{13}C$ (‰)
Al Gacel MV	D10-R3	Coral skeleton	1	2.35	−5.58
		Authigenic carbonate	2	3.37	−20.07
			3	3.60	−26.68
			4	3.70	−20.79
			5	3.45	−22.43
			6	3.80	−20.70
		Coral skeleton	7	3.28	−2.23
		Authigenic carbonate	8	3.83	−25.16
			9	3.63	−25.29
			10	3.91	−18.38
			11	3.60	−24.18
			12	3.55	−25.34
			13	3.56	−25.15
		Coral skeleton	14	3.50	−2.09
		Authigenic carbonate	15	3.92	−21.89
	D10-R7	Authigenic carbonate	21	2.90	−26.36
			22	3.15	−28.77
			23	2.94	−22.91
			24	2.67	−21.13
			25	2.37	−24.70
			26	2.56	−23.60
	D11-R8	Coral skeleton	16	1.49	−4.91
			17	2.13	−2.99
			18	1.74	−4.22
		Authigenic carbonate	19	5.60	−14.82
			20	5.55	−14.74
Northern Pompeia Coral Ridge	D03-B1	Coral skeleton	1.1	−0.38	−7.93
			1.2	−0.86	−7.77
			1.3	−0.51	−7.35
			1.5	1.15	−5.26
			1.4	−1.03	−8.08
			1.6	0.69	−5.96
			1.7	0.54	−6.42

758

Table 4. Continued

Location	Sample	Origin of the carbonate	Identification number in Fig. 7	$\delta^{18}O$ (‰)	$\delta^{13}C$ (‰)
Northern Pompeia Coral Ridge	D03-B1	Coral skeleton	3.1	1.59	−2.08
			3.2	−0.31	−6.27
			3.3	−0.89	−6.78
			3.4	−0.94	−6.73
			3.5	1.84	−2.21
			3.6	2.26	−1.39
			3.7	1.74	−2.87

760

761 **Table 5.** Stable carbon isotopic composition ($\delta^{13}C$) of selected lipid biomarkers (in **Figure 10**). (*) Please note
762 that crocetane in D11-R8 coelutes with phytane. n.d. = not detected.

Compound	D10-R7 (‰)	D11-R8 (‰)
n-C_{17}	n.d.	−33.0
n-C_{18}	n.d.	−31.8
n-C_{19}	n.d.	−31.1
n-C_{20}	n.d.	−30.8
n-C_{21}	n.d.	−31.5
n-C_{22}	n.d.	−31.7
Crocetane*	−101.2	−57.2
PMI	−102.9	−74.3

763
764
765
766
767
768
769
770
771
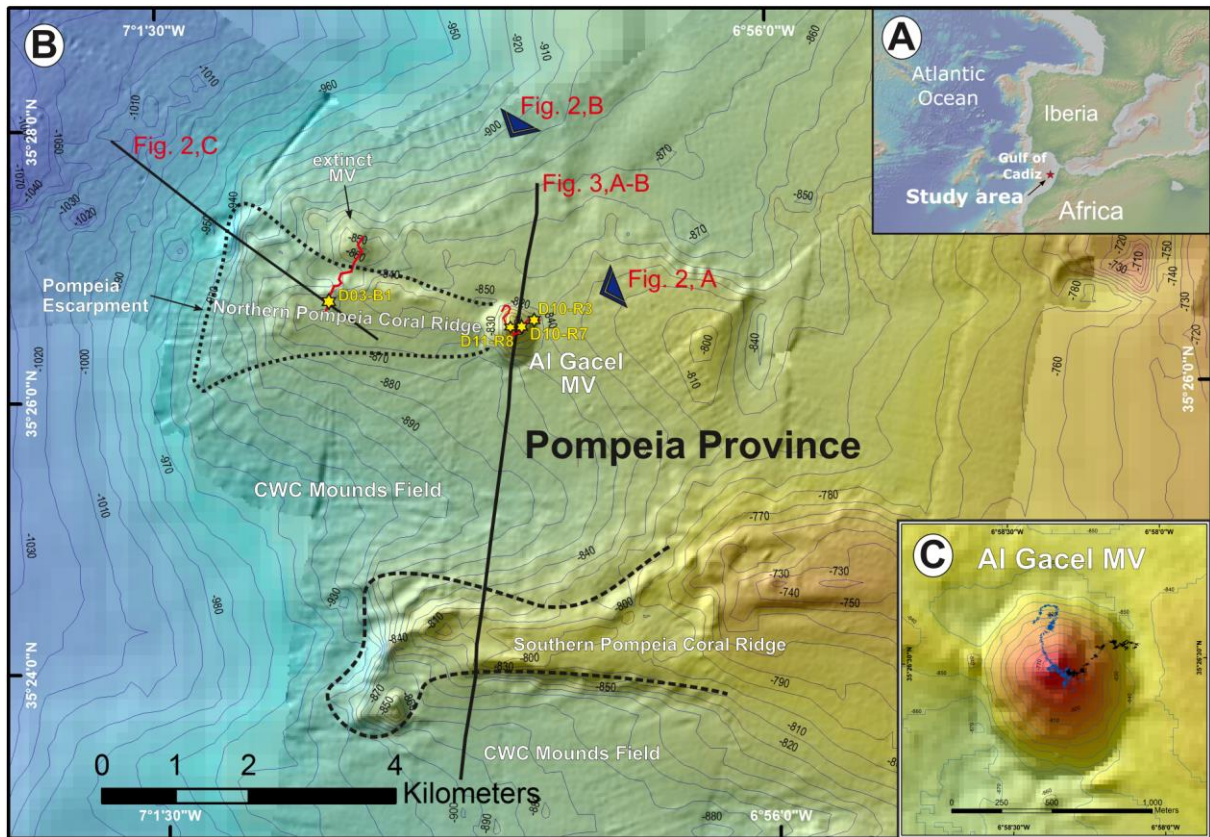
Figure 1. Bathymetric map of the study area. **A**: location of the Gulf of Cádiz between Spain, Portugal and Morocco. The study area is marked with a red star; **B**: the Pompeia Province including its different morphological features. Red lines indicate ROV-paths, yellow stars mark sampling sites; **C**: detailed map of the Al Gacel MV including pathways of Dive 10 and 11 (black and blue lines, respectively). Further details of the area are provided in **Figs. 2** and **3**.
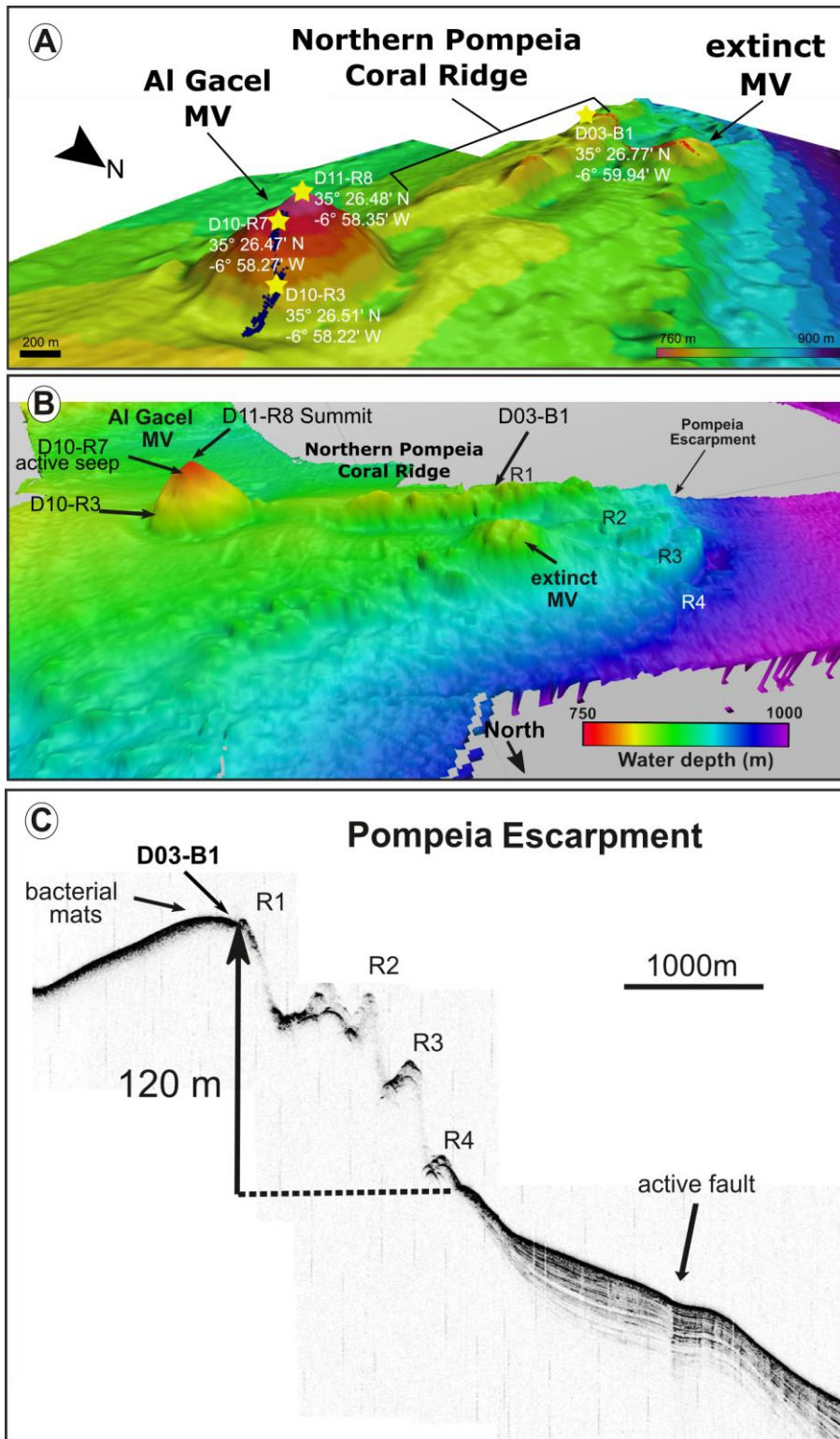
Figure 2. Bathymetric and seismic maps showing morphological features in northern Pompeia Province. **A–B**: bathymetric maps showing the Al Gacel MV, the Northern Pompeia Coral Ridge and the extinct MV. Yellow stars mark sampling sites. **C**: ultra-high seismic profile of the Pompeia Escarpment, westwards of the Northern Pompeia Coral Ridge.
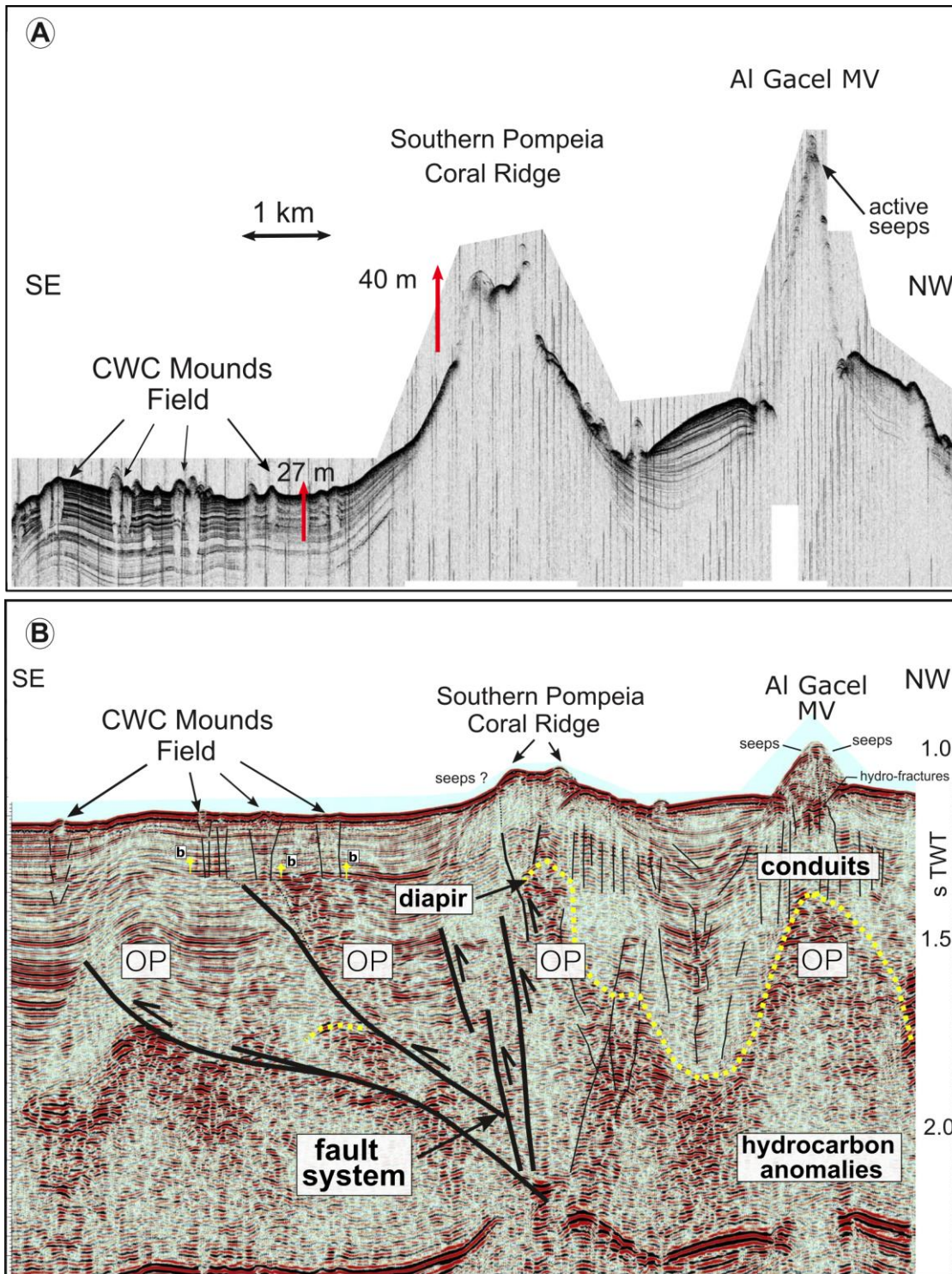
784

785 **Figure 3.** Ultra-high resolution (**A**) and multichannel (**B**) seismic profiles showing geological features in southern

786 Pompeia Province. Note mud diapirism has been described in this area (Vandorpe et al., 2017). OP = overpressure

787 zone.
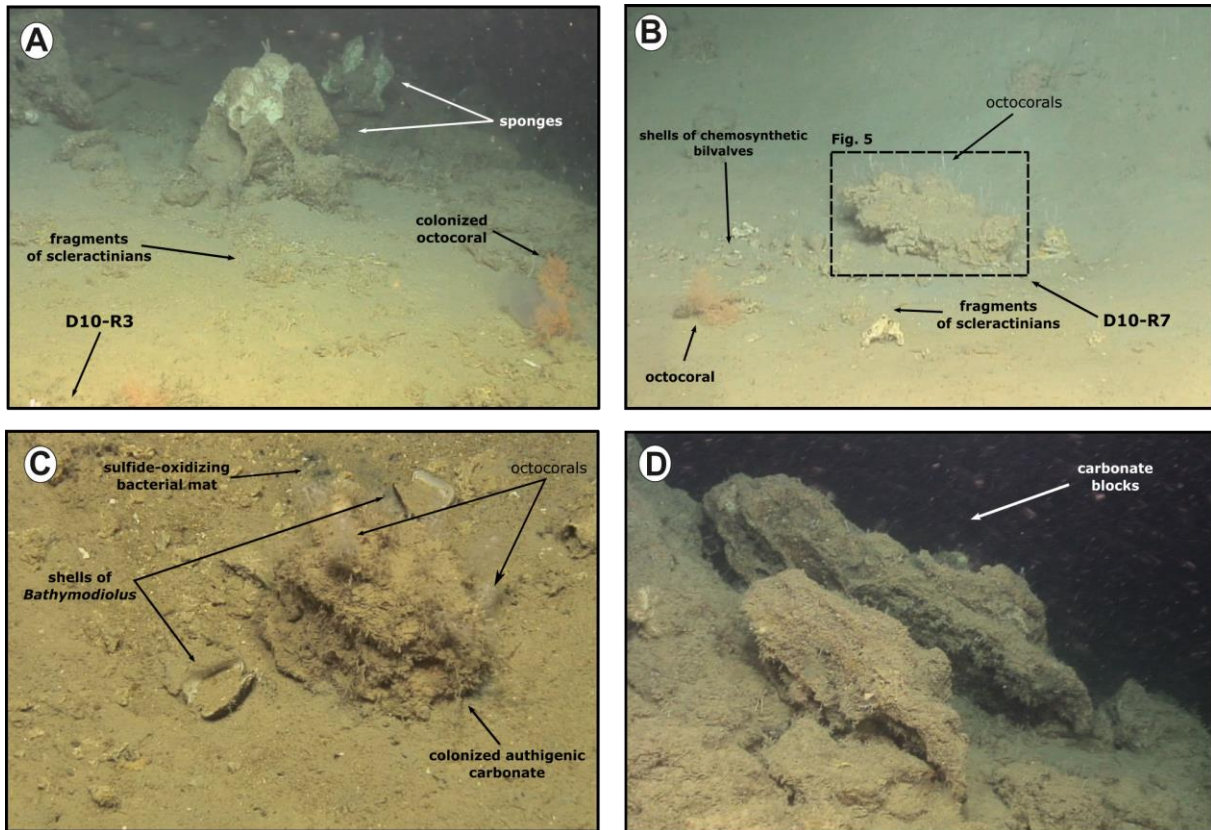
Figure 4. ROV still frames from the Al Gacel MV (Dives 10 and 11). **A**: eastern side of the volcano, displaying a field of sponges, corals and carbonates; **B–C**: active pockmark sites on the east side of the volcano, displaying authigenic carbonate surrounded by shells of chemosynthetic bivalves, fragments of scleractinian and octocorals, as well as sulfide-oxidizing bacterial mats; **D**: metric-sized carbonate blocks located in a slope at the summit of the volcano.
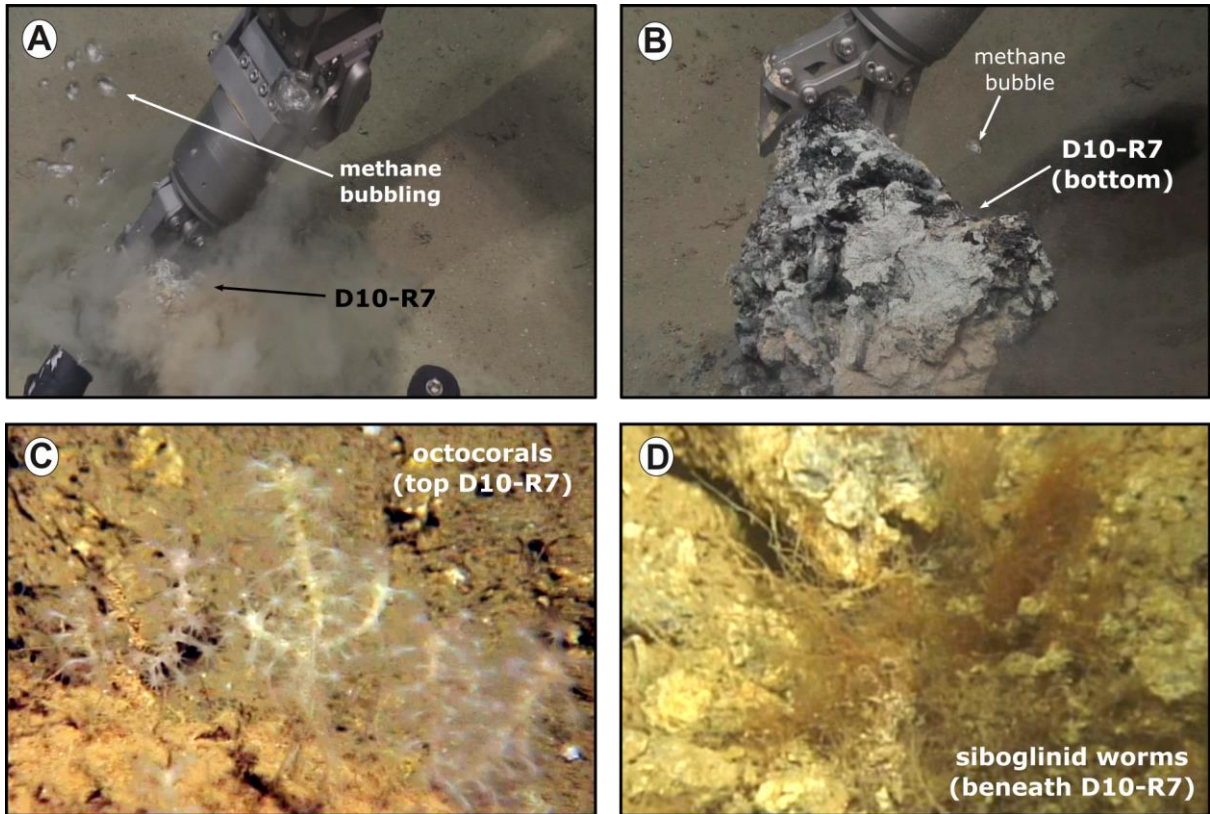
Figure 5. ROV still frames from the active pockmark site shown in **Fig. 4**, **B**. **A–B**: release of bubbles while sampling; **C**: detailed photograph of the octocorals on top of the carbonate; **D**: detailed still frame from siboglinid worms beneath the carbonate.
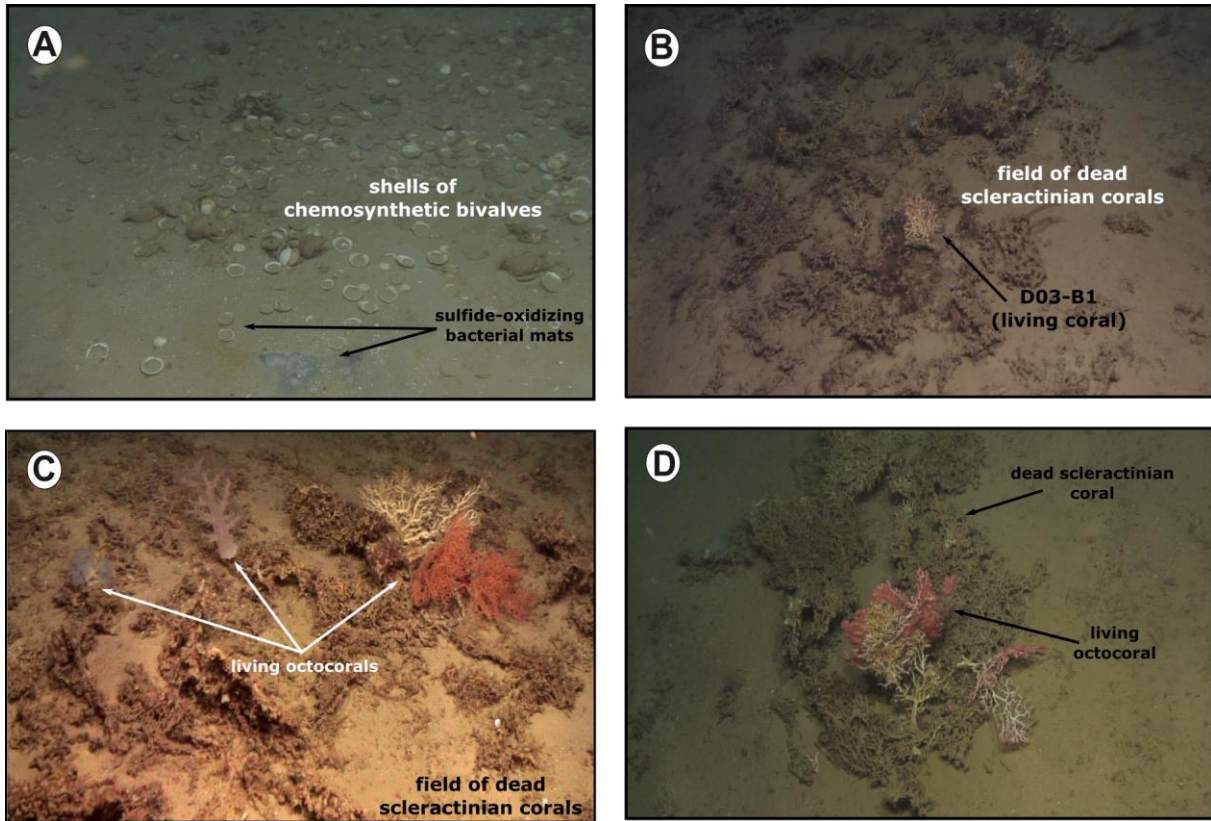
Figure 6. ROV still frames from the Northern Pompeia Coral Ridge and extinct MV (Dive 03), where there is currently a diffused seepage of fluids. **A**: abundant shells of chemosynthetic bivalves with sulfide-oxidizing bacterial mats at the western site of the Northern Pompeia Coral Ridge; **B–D**: field of dead scleractinian-corals colonized by living corals; **D**: still frame from the extinct MV.
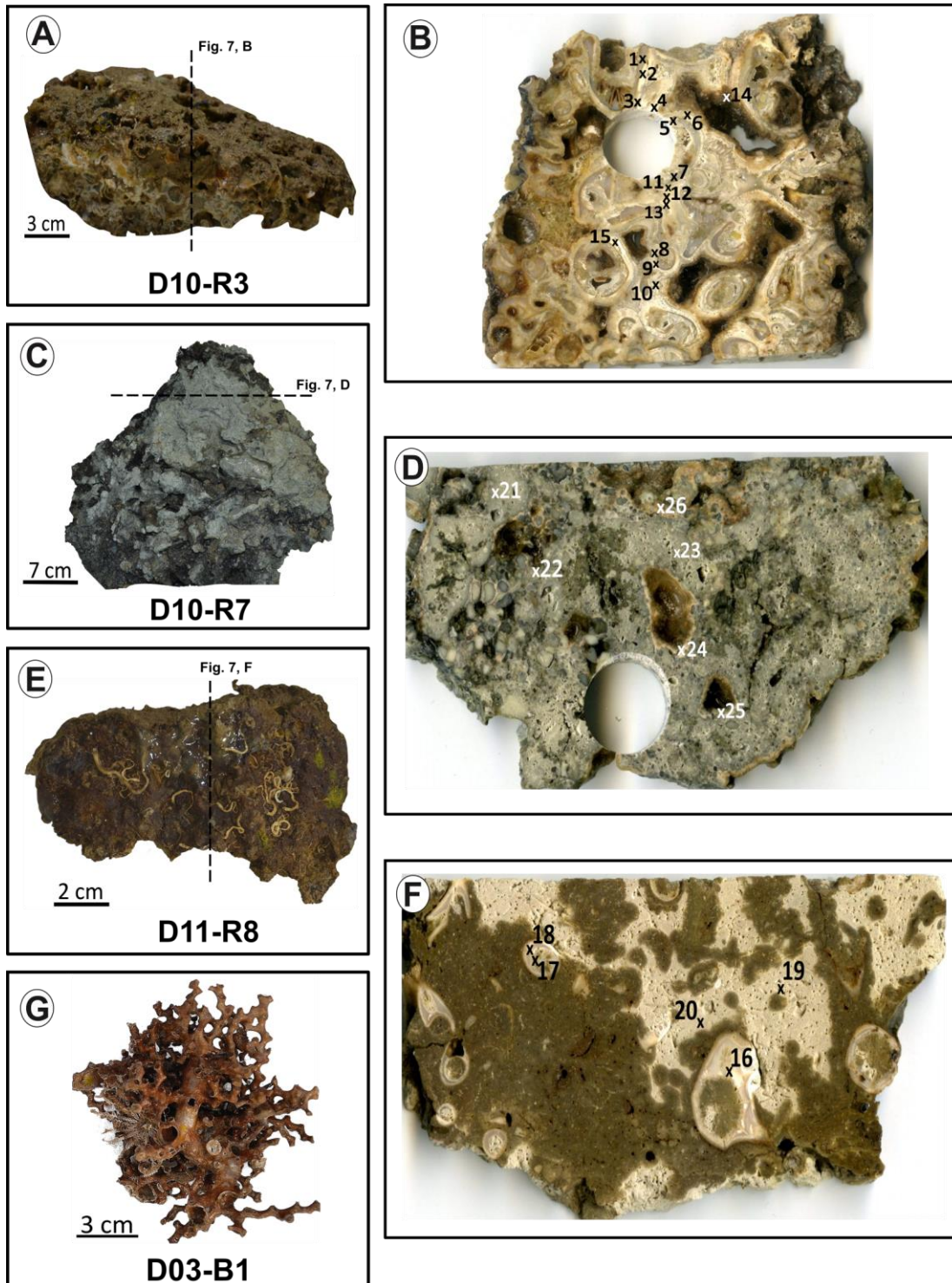
Figure 7. Photographs of analyzed samples including sampling sites for stable carbon and oxygen isotope (δ^{13}C, δ^{18}O) analysis (crosses with numbers). Values of the stable isotopic analyses are found in **Table 2**. **A–B**: D10-R3 carbonate with embedded corals; **C–D**: D10-R7 carbonate with strong H_2S odor; **E–F**: D11-R8 carbonate with embedded corals; **G**: D03-B1 scleractinian-coral fragment, *Madrepora oculata*. Please note that we cannot determine whether the corals were alive or dead the time they were buried by the carbonate.
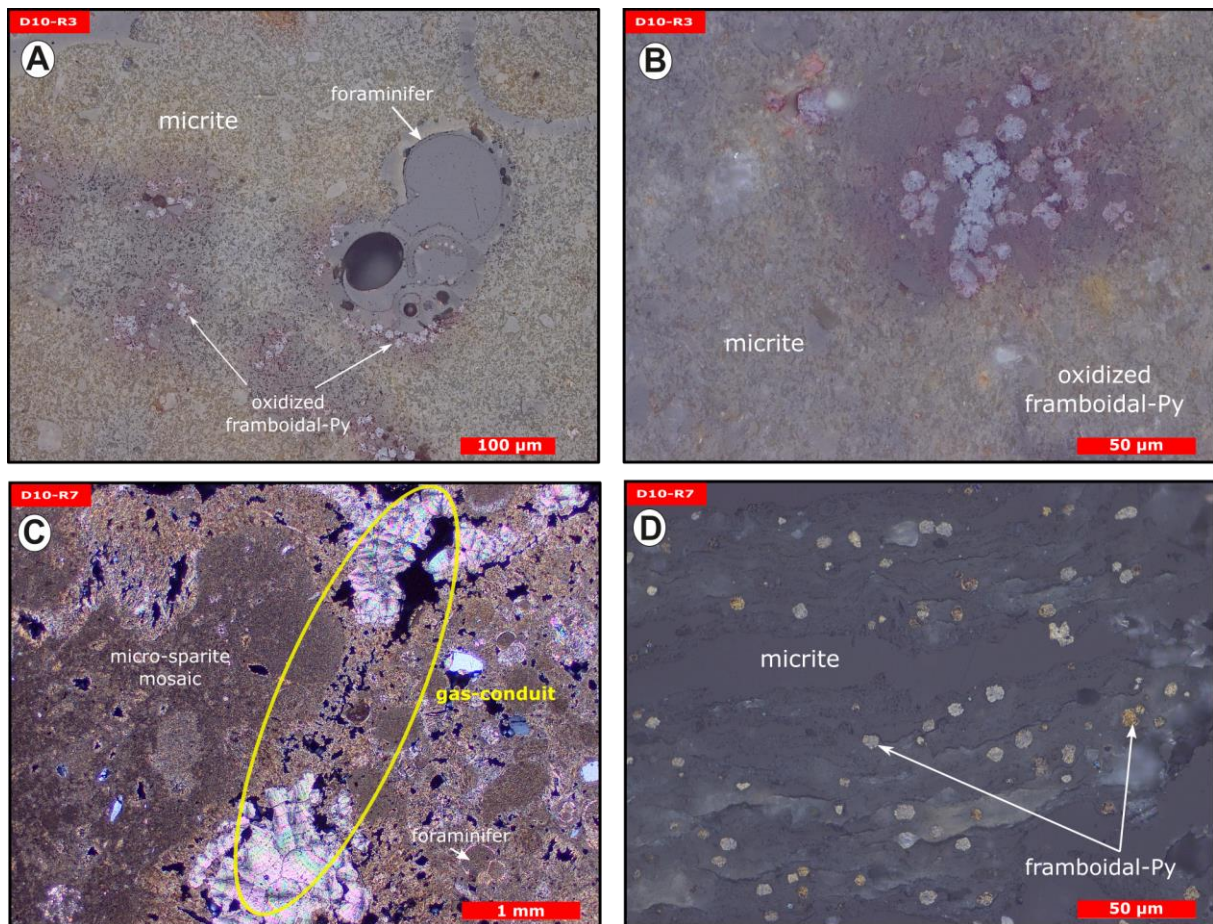
Figure 8. Thin section photographs of MDACs. **A–B**: D10-R3 consisting of a micritic matrix with scattered foraminifers and oxidized framboidal pyrites (reflected light); **C–D**: D10-R7 consisting of micritic and micro-sparitic carbonate with abundant unaltered framboidal pyrites (C, transmitted light; D, reflected light). Please note open voids which represent potential pathways for fluid seepage (yellow circle in C).
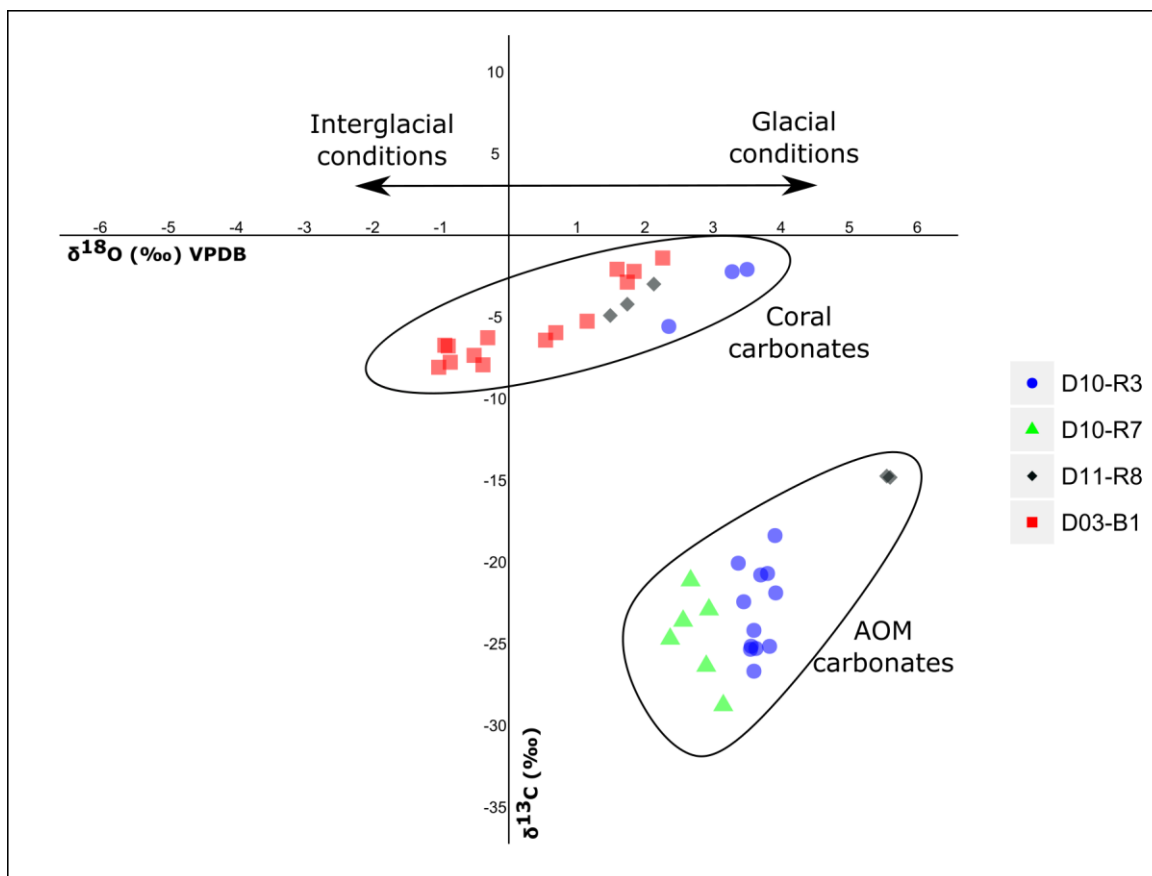
Figure 9. Stable carbon and oxygen isotopes (δ^{13}C, δ^{18}O) of samples from the Al Gacel MV and the Northern Pompeia Coral Ridge (see **Figure 3** for precise sampling points).
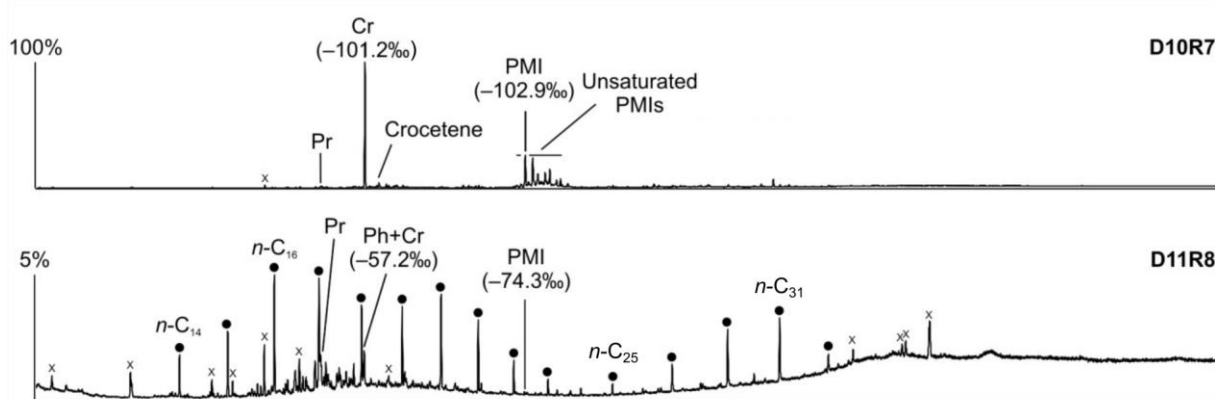

Figure 10. Total ion current (TIC) chromatograms of the analyzed samples. Isotopically depleted acyclic irregular isoprenoids such as Cr and PMI are typically found in settings influenced by the anaerobic oxidation of methane (AOM). Pr = pristane; Ph = phytane; Cr = crocetane; PMI = 2,6,10,15,19-pentamethylicosane; dots = n-alkanes; crosses = siloxanes (septum or column bleeding). Percentage values given on the vertical axes of chromatograms relate peak intensities to highest peak (Cr in D10-R7).

838
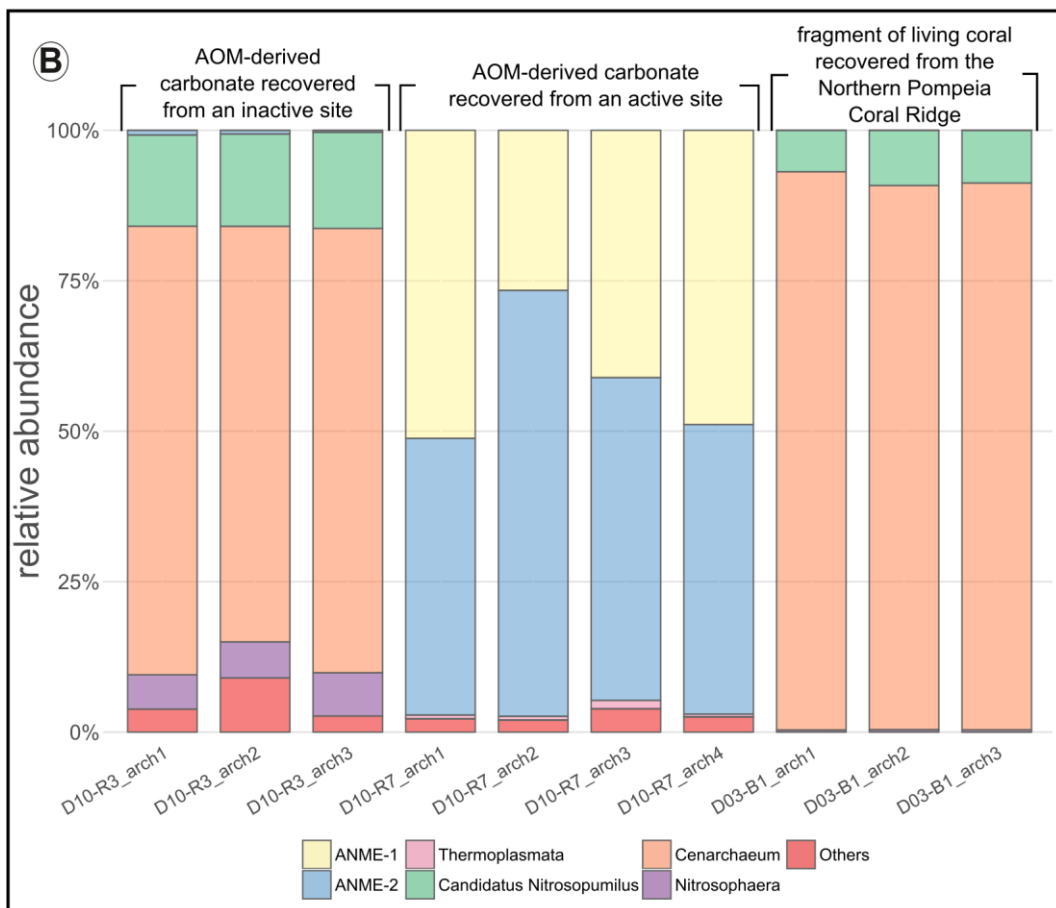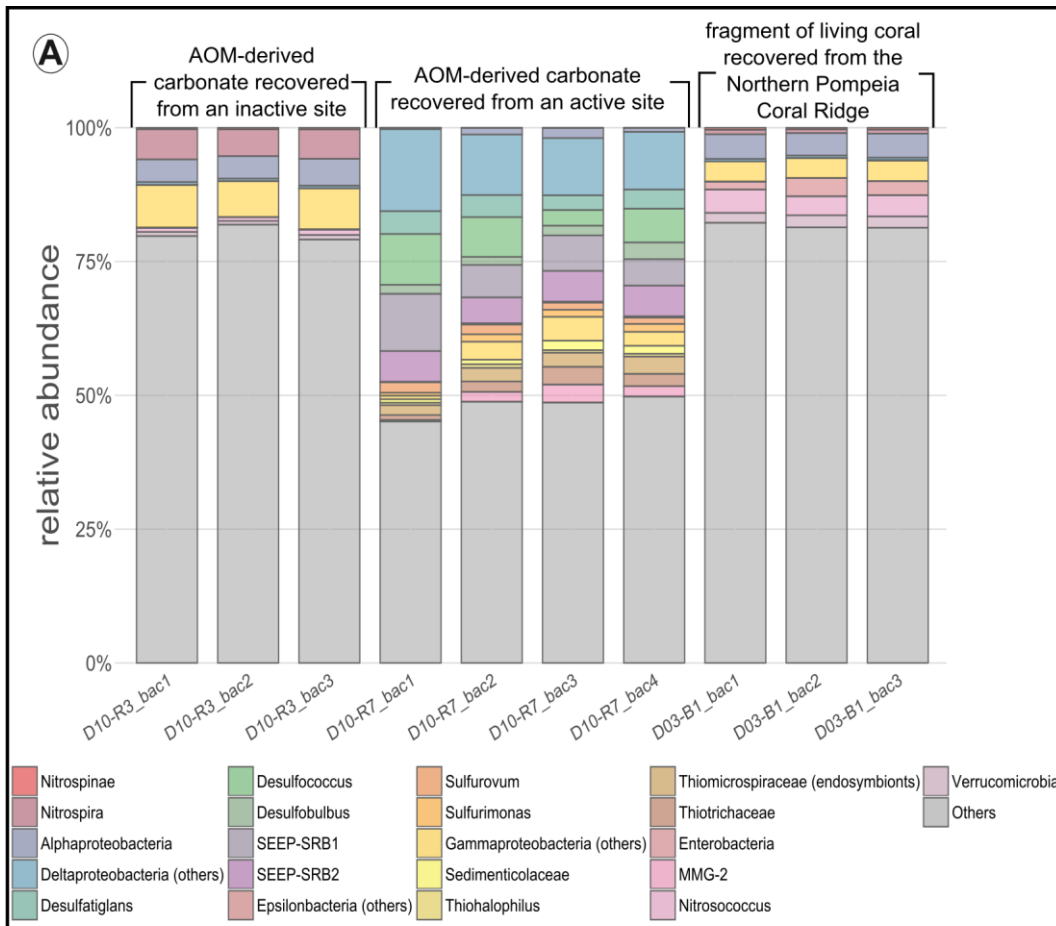
839   **Figure 11**. Bar chart representing relative abundances of prokaryotic taxa detected in each sample. **A**: bacterial

840   taxa; **B**: archaeal taxa. In "others" aggrupation is included taxa related to ubiquitous organism normally found in

841   sea- and seepage-related environments, and unclassified organisms. Number of reads per taxa detailed in **Table**

842   **S1** (bacteria) and **Table S2** (archaea).
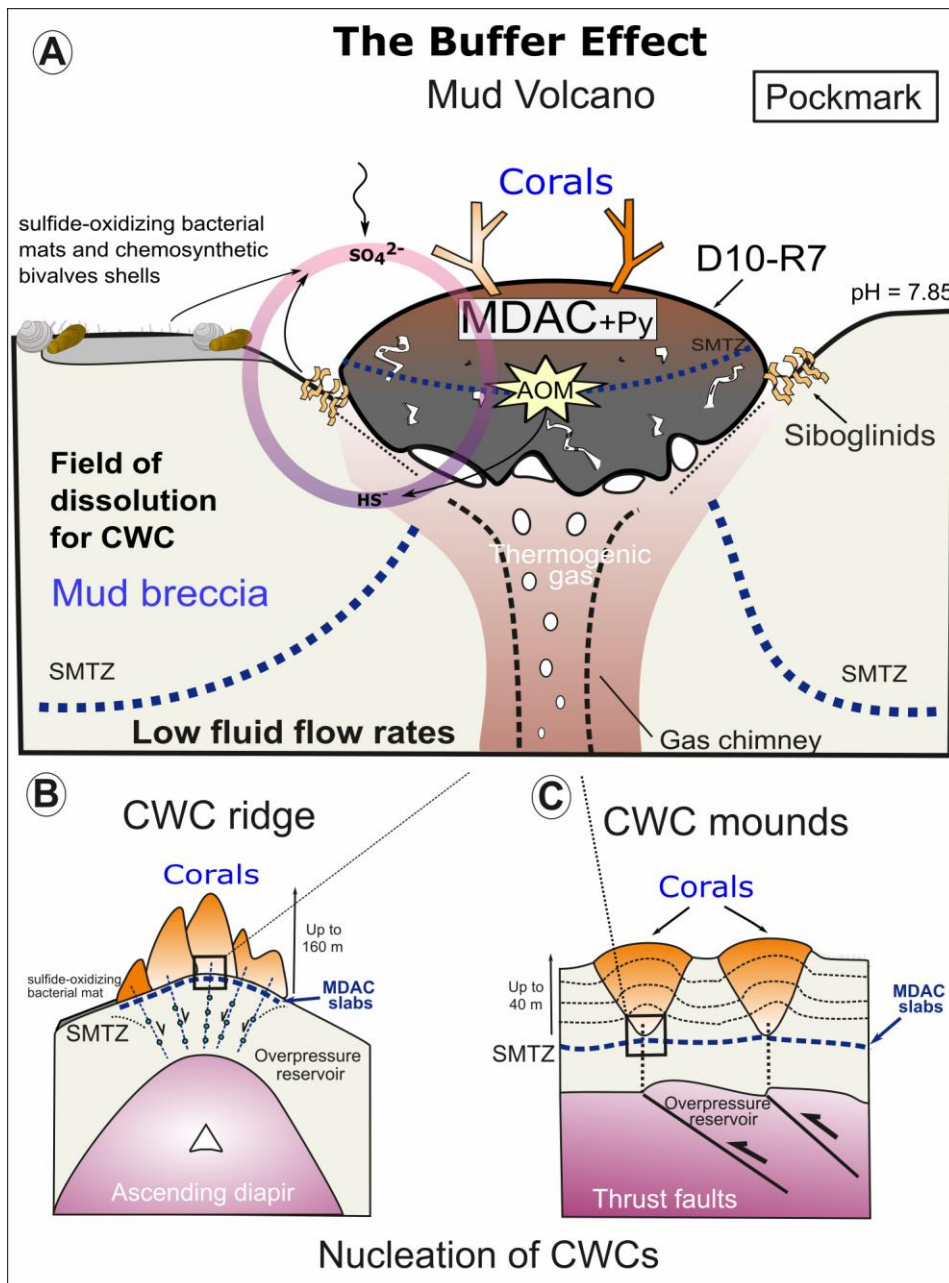
Figure 12. The buffer effect model. **A**: Buffer effect at pockmark sites (e.g. sampling site of D10-R7) where carbonates are formed directly on the bubbling site acting as a cap; **B**: Buffer effect at diapiric ridges where MDAC slabs are formed on the base of the ridge; **C**: Buffer effect at coral mounds where MDAC slabs are formed in deeper layers of the sediment. Py = pyrite, SMTZ: sulfur-methane transition zone.